Macroscopic **Q**uantum **R**es**o**nators (**MAQRO**)

[Testing quantum and gravitational physics with massive mechanical resonators]

Proposal for an **M-class mission** with possible launch in 2022

submitted by
R. Kaltenbaek[1], G. Hechenblaikner[2], N. Kiesel[1], U. Johann[2], and M. Aspelmeyer[1]

(1) Quantum Optics, Quantum Nanophysics and Quantum Information
Faculty of Physics, University of Vienna
Austria
(2) EADS Astrium, Friedrichshafen, Germany

contact details:

Group Prof. Aspelmeyer
Quantum Optics, Quantum Nanophysics and Quantum Information
Faculty of Physics, University of Vienna
A-1090 Wien
Austria

phone: +43 (0) 1 4277 72531
fax: +43 (0) 1 4277 9512
e-mai: aspelmeyer-office@univie.ac.at

1 Executive Summary

What are the fundamental physical laws of the universe?
The laws of quantum physics challenge our understanding of the nature of physical reality and of space-time and suggest the necessity of radical revisions of their underlying concepts. Experimental tests of quantum phenomena that involve massive macroscopic objects, such as quantum superpositions, provide novel insights into these fundamental questions. MAQRO is a unique optical space experiment that allows to enter a new parameter regime of macroscopic quantum physics and hence to address some of the most important questions in our current understanding of the basic laws of gravity and of quantum physics of macroscopic bodies.

MAQRO – fundamental science and technology pathfinder
MAQRO unites two experiments: DECIDE (Decoherence in Double-Slit Experiments) and CASE (Comparative Acceleration Sensor):
The main scientific objectives of MAQRO, which will be realized by the experiment DECIDE, is to test the predictions of quantum theory in a hitherto inaccessible regime of quantum superpositions of macroscopic objects that contain more than 10^{10} atoms. This is achieved by a new experimental approach that combines techniques from quantum optomechanics with optical trapping of macroscopic dielectric particles. MAQRO operates in a parameter regime, in which various suggested alternative models to quantum theory would become visible. These models have been suggested to harmonize the paradoxical quantum phenomena both with the classical macroscopic world (by Ghirardi, Rimini, Weber and Pearle) and with our current notion of Minkowski space-time (by Penrose, Karolyhazy and Diosi). MAQRO therefore establishes a direct investigation of the underlying nature of quantum reality and space-time.
The second scientific objective of MAQRO, realized by the experiment CASE is to demonstrate the performance of a completely new technology for drag-free sensing that is based on optical trapping of microspheres, as is used in DECIDE. This technology demonstrator will at the same time serve as a test bench for the weak equivalence principle with a test mass difference of 7 orders of magnitude.

MAQRO – a unique environment for macroscopic quantum experiments
In earth-based experiments the ultimate limitation for observing macroscopic quantum superpositions is localizing decoherence through interaction with the environment, in particular through collisions with background gas and through scattering and emission of radiation. The spacecraft design of MAQRO allows to operate the experimental platform at a unique combination of low pressure ($< 10^{-12}$ Pa) and low temperature (< 40K), which is necessary to suppress quantum decoherence phenomena to a level that the effects of alternative models to quantum theory become experimentally accessible.

MAQRO – an LTP upgrade
MAQRO capitalizes on the current developments in optical space technology, specifically on the design of the LISA technology package LTP. The basic experimental platform, the spacecraft, the launcher, the ground segment and the orbit (L1) are identical to LTP. An alternative mission in HEO configuration is also feasible. This would not only allow simultaneous tests of the equivalence principle but would also fit well into the scope of ACES/Pharao, another fundamental science mission proposed within the Cosmic Vision program. It might well be feasible to combine these experiments on one spacecraft. Modifications to the LTP design are the inclusion of an optical resonator and a different mounting of the propulsion system to achieve the required low vacuum level. The

technological readiness level of the optical cavity setup and of the vacuum platform is 3-5, for all other elements it is 6-9 because of the full technological heritage from LTP. An implicit strength of MAQRO is that it is comprised of two independent experiments, DECIDE and CASE, each of which could, in principle, be combined on the same spacecraft with other missions that have similar requirements in precision and orbit.

Alternative scenario due to modular concept

The alternative MAQRO mission scenario of a highly elliptical (polar) earth orbit lends itself in principle to expand the scientific yield of the project in a complemetary natural way by adding a precision optical clock and radio science experiment to the payload, with the objective to measure the gravitational time dilation with unprecedented accuracy within a widely variing gravitational potential range. Similar scenarios have been proposed recently, e.g. for the first ESA Cosmic Vision call (EGE:Einstein Gravity Explorer, S.Schiller et al., 2007). The experiment features a precision optical ion clock on board, a frequency comp converter and an optical or microwave link to ground stations for local clock comparison, similar to the ACES/Pharao project recently in implementation phase for operation on the ISS. The experiment technology required is in parts similar to the one employed for MAQRO experiments and has the potential to master a maturity level for embarking a mission on the envisioned time scale. The recources required on board we estimate to be about additional mass and power of 150 kg and 200W, respectively. While the added experiment puts additional constraints on orbit selection, (e.g. ground station contact), the reduced delta v requirements of this orbit as compared to a halo orbit at L1 provides aditional mass margins in the order of the requirements, without drastically changing the baseline mission budgets. No detailed analysis of this scenario has been performed yet, however.

2 Introduction

Testing the predictions of quantum theory on macroscopic scales is one of today's outstanding challenges of modern physics and addresses fundamental questions on our understanding of the world. Specifically: will the counterintuitive phenomena of quantum theory prevail on the scale of macroscopic objects? This is at the heart of the so-called “quantum measurement problem”, also known as Schrödinger’s cat paradox. Another question is whether quantum superposition states of massive macroscopic objects are consistent with our notion of space-time or whether quantum theory will break down in such situations? This might possibly open up a new route for experimental investigations of quantum gravity. Questions of this kind, i.e. at the interface between quantum laws and the macroscopic world and gravity, address the basic building blocks of our world view and cannot be answered with our present state of knowledge.

The recent developments in research on massive mechanical resonators promise access to a completely new parameter regime for macroscopic quantum experiments, in particular in combination with quantum optical control techniques. These devices allow the study of the collective center-of-mass motion of massive objects that contain up to 10^{20} atoms and that span the size range from hundreds of nanometers in the case of nano-electro-mechanical or nano-opto-mechanical systems (NEMS/NOMS) to tens of centimetres in the case of gravitational wave antennae. Within a very short time scale of only a few years research on mechanical systems has generated a new interdisciplinary community of scientists who seek to achieve control over mechanical quantum states. Quantum optics provides a well-developed toolbox to generate, control and manipulate quantum states of a mechanical system This developing field of quantum-opto-mechanics provides - aside from numerous novel sensing and actuation technologies at and beyond the quantum limit - a unique opportunity to

generate superposition states of massive objects by opening up a completely new perspective to macroscopic quantum experiments.

The case for space
Space offers a particularly advantageous environment to push such macroscopic experiments to their ultimate performance limits. This includes explicitly the pressure and temperature of the environment, which can be kept significantly below the achievable parameters for ground-based experiments, combined with the possibility of long observation times (~10 seconds) during which the dielectric spheres are not confined in an optical potential but propagate in free fall.

Heritage
The specific optomechanical systems implemented by MAQRO is a dielectric sphere that is trapped and controlled inside an optical cavity. This allows a direct adaptation of the LISA technology package LTP, which already contains many of the core elements for quantum-opto-mechanical experiments. MAQRO therefore makes maximal use of scientific and technological heritage of existing space missions (see below).

3 Scientific objectives and requirements

3.1 Science Goals

The proposed mission hosts two separate experiments – DECIDE will be a novel test of fundamental physics, while CASE will use similar technology but for a technical comparison of a new type of accelerometer with a well-established electrostatic accelerometer as it is used in various space missions that either have been performed already or will be performed in the near future:

- CASE (**C**omparative **A**cceleration **SE**nsor)
  an Onera-type capacitative inertial sensor will be used for high-precision drag-free control of the spacecraft. A novel accelerometer that is based on a fundamentally different design will be operated in parallel to compare the performance of the new sensor with that of a well-established one. Data from this mission will enable a promising technology to be used in future high-precision tests of gravitation and/or for attitude and orbit control.
- DECIDE (**DEC**oherence **I**n **D**ouble-slit **E**xperiments):
  this experiment aims at testing the predictions of quantum theory in a parameter regime where gravity becomes a relevant factor. By combining novel techniques of preparing mechanical resonators in non-classical states with the well-established technique of optical levitation, we propose double-slit experiments that will allow to directly test the predictions of quantum theory against those of extensions to quantum theory that predict a collapse of quantum states for macroscopic systems due to, e.g., gravitation.

The scientific objectives and requirements of these two experiments will be described in detail in the following subsections.

3.1.1 CASE – Comparative Acceleration SEnsor

One of the foundational principles of Einstein's theory of relativity is the equivalence principle (EP). Even before Einstein, however, Galileo and later Newton tested the universality of free fall experimentally. In particular, Newton wanted to assure that one of the principles in his theory, the equivalence of inertial and gravitational mass, was experimentally founded. In the language of general relativity, the equivalence principle deals with local experiments, i.e., experiments that happen on a small enough scale where tidal forces can be neglected, such that the metric can locally be assumed to be flat (Minkowski metric). One distinguishes between the weak and strong equivalence principle:

- *Weak Equivalence Principle:* all test particles experience the same acceleration in a gravitational field, independent of their constituents and their rest mass.
- *Strong Equivalence Principle:* no experiment, including experiments involving gravitational forces between various constituents of the system, can distinguish between a local reference frame in a gravitational field and an accelerated reference frame in a flat space-time.

The form of the equivalence principle used by Einstein is essentially equivalent to the weak equivalence principle; it states that the outcome of any local experiment not involving gravitation neither depends on the velocity of the laboratory nor on its position in space-time.

Motivation

Something that is implicit in the equivalence of free fall for materials of differing composition is that the acceleration in a gravitational field is independent of the interactions between the various constituents of the test mass. In extensions of the standard model of physics like, e.g., string theory, which aim at unifying the gravitational interaction with the other fundamental interaction, the description of the graviton as a spin-2 particle leads to an additional scalar field [1]. Depending on the specific model and the parameters chosen, this can lead to corrections to the inverse-square law of gravity over short distances [2,3], or to a violation of the equivalence principle or a variation of physical constants over time [4]. With MICROSCOPE [5], a promising mission to test the EP to an accuracy of 10^{-15} is soon to be launched. Like in the proposed STEP mission, the inertial sensor in MICROSCOPE is based upon electrostatic force measurements. This is the working principle of ONERA inertial sensors, which are well established and have been used in various space missions (e.g. in GOCE, ASTRE, STAR and in Space Shuttles).

Recently, it has been suggested it should be possible to dramatically improve the accuracy of experimental tests of the inverse-square law over short distances by using optically levitated nanospheres. In our proposal for a test of the equivalence principle, we want to demonstrate that optical trapping might also prove to be a versatile and precise new tool to measure accelerations as a supplement to determining acceleration via electrostatic force measurements.

Current status and planned experiments

While all experiments up to now have confirmed the equivalence principle [2,6,7], possible extensions of the standard model of physics predict a violation of the equivalence principle [4] in parameter regimes that are now within reach of experimental tests. Recent years have

seen an increasing interest in precision tests of the equivalence principle [2,6]. By now these tests have reached an accuracy that is difficult to enhance in Earth-based experiments due to various noise sources of, e.g., human and seismic origin that are inevitably limiting such experiments. Already in 1970, Chapman and Hanson proposed a space-based test of the equivalence principle with a fractional accuracy of up to $\delta a/a = 10^{-14}$ [8]. This vision finally led to the proposal of STEP, which aims at an accuracy of $\delta a/a = 10^{-18}$ [9]. While at the moment it seems not clear if and when STEP, as the most ambitious envisioned EP test so far, will be launched, the smaller scale mission MICROSCOPE is supposed to be launched in the near future. It aims at an accuracy of 10^{-15} [5], which is better than the sensitivity of 10^{-12}, below which one can expect deviations from general relativity [4].

Comparison with other missions

In the experiment CASE, which is one of the two experiments hosted by MAQRO, two accelerometers of very different architecture will monitor any accelerations that two test bodies will experience during the propagation of the space craft along its trajectory. One of the inertial sensors will be an electrostatic sensor, which we will, for now, assume to be identical to the GRADIO accelerometer as it is used in the GOCE mission [10]. Under the conditions in that mission, this sensor allows for inertial measurements with a resolution of up to $4\times10^{-13}\,\mathrm{ms^{-2}Hz^{-1/2}}$ in the frequency bandwidth between 5×10^{-3} Hz to 0.1 Hz [10]; we will assume a similar performance in the proposed mission. The proof mass in this sensor is a Platinum-Rhodium alloy with a mass of 320 g.
The second sensor is of a new type that is based on monitoring the position of a dielectric microsphere within an optical potential. We aim at reaching a level of accuracy with this sensor similar to the accuracy of the electrostatic sensor. Given the vast difference in mass between the microsphere (on the order of 10^{-8} kg) and the proof mass in the electrostatic sensor (320 g) a measurement of the differential acceleration between these two sensors will be a highly accurate test of the universality of free fall. In addition, the architecture of this new optomechanical sensor will allow for exchanging the dielectric sphere in the optical potential with other dielectric spheres of different mass and composition.

3.1.2 DECIDE – Testing Quantum Mechanics against Macrorealistic Theories

Quantum theory is one of the most successful theories known today. But although it has been confirmed over an impressive parameter range in every experiment performed so far, its axioms remain to be purely mathematical and open to a variety of interpretations that are, up to now, more or less a question of taste. At the same time the predictions of quantum mechanics seem to be in blatant contradiction to our everyday experience, where objects are always in distinct states that can be verified without disturbing the system under investigation, whereas we confirm concepts of quantum theory like superposition and the interference of probability amplitudes every day in laboratories around the world.

Is there an essential difference between macroscopic and microscopic objects, and if there is, what brings about the transition between these two distinct realms, and when does it occur?

If quantum theory is correct, then any system, independent of its size and complexity, can be brought into a state that is called a quantum superposition where a physical system is, in a

way, in two distinct states at once. Schrödinger treats this in his famous gedankenexperiment, where a cat is brought into a superposition of being dead and alive. According to quantum theory, this is possible in principle as long as the system in question is isolated completely from its environment such that nobody could possibly know whether the system is in one state or the other except by performing a measurement on the system itself.
Several theoretical models have been put forward that propose to modify the laws of quantum theory to introduce a collapse of the wavefunction for complex and/or massive objects or objects that are distributed over large distances [11-16] . We call these models *macrorealistic*, and in this proposal, we will concentrate on three models:

- **K-Model**
  In this model by Karolyhazy [11], the uncertainty principle of quantum theory leads to uncertainties in the metric and as a result to the collapse of the wavefunction for massive particles and/or large spatial extensions.
- **Penrose Model**
  Penrose [15] suggests that a superposition of massive objects would lead to a superposition of different space-time structures, which is incompatible with the realistic character of the space time and thus leads to a collapse of wavefunctions for massive particles for large spatial extensions.
- **GRW Model**
  This is a generic model [12,13,16] that does not give a specific mechanism for the collapse of the wavefunction. This model depends on two parameters that determine the level of decoherence for particles consisting of many constituents or superpositions that extend over large spatial distances.

The **scientific goal of DECIDE** is to perform decisive experimental tests between the predictions of quantum theory and those of the macrorealistic theories described above. It will do so by attempting to prepare optically trapped nanospheres in quantum superposition states that should, according to the macrorealistic above decohere much quicker than predicted by quantum theory. The level of coherence or decoherence of the prepared superposition states can be determined by measuring the visibility of an interference pattern equivalent to that observed behind a double slit. If the observed visibility falls off only with the slower decoherence rate predicted by quantum theory, it is possible to rule out those macrorealistic models that predict a much faster decoherence.
The **central requirement** in order to perform such a test is that quantum theory predicts that we are still able to observe high visibility interference fringes while the theories we test against do not. In particular, that means that the effects of those mechanisms that lead to decoherence even according to quantum theory are minimized to a level where they are either negligible or much slower then the decoherence due to macrorealistic descriptions.

Decoherence according to quantum theory

As we have mentioned earlier, decoherence in quantum mechanics occurs due to information that can be gained from a system's environment about the actual state of the physical system we want to prepare in a superposition. There are many ways in which a physical system can interact with its environment. We will concentrate on those that will be the dominating cause for decoherence if we do not properly choose the experimental parameters:

- **Decoherence due to collisions with background gas**
  This mechanism depends on the density of the background gas, the velocity of the gas particles, and on the scattering cross section of our physical system.

- **Scattering of blackbody radiation**
  This depends on the temperature of the surrounding environment, and on the scattering cross section of the nanosphere, which depends on the particle's dielectric properties and on the particle's size.
- **Emission of blackbody radiation**
  Depending on the internal temperature of the nanosphere, on its dielectric properties, and on its size, the particle will emit blackbody radiation that can localize it and lead to decoherence.
- **Absorption of blackbody radiation**
  This depends on the particle's dielectric properties, its size, and on the temperature of the surrounding environment.

Observation of double-slit interference

The way we choose to prepare the nanosphere in a quantum superposition is the following. First we prepare it in its ground state of motion. This is necessary in order to have the particle localized as well as possible and in a known quantum state. Then we free the particle of its optical trap, and the particle's wavefunction will expand for some time τ_1. After that time, we shoot a very tightly focused pulsed laser beam through the middle of the wavepacket. If the particle scatters photons from the laser, we start the experiment again. If it does not scatter any photons, the nanosphere now could be either to one or the other side of the laser beam. Once this preparation succeeds, we let the wavefunction expand further, for a time τ_2. As the two remaining parts of the wavefunction start to overlap again, they will interfere. If we measure the position of the particle, and if we repeat that procedure many times, then the distribution of the measured particle positions will form a double-slit interference pattern.

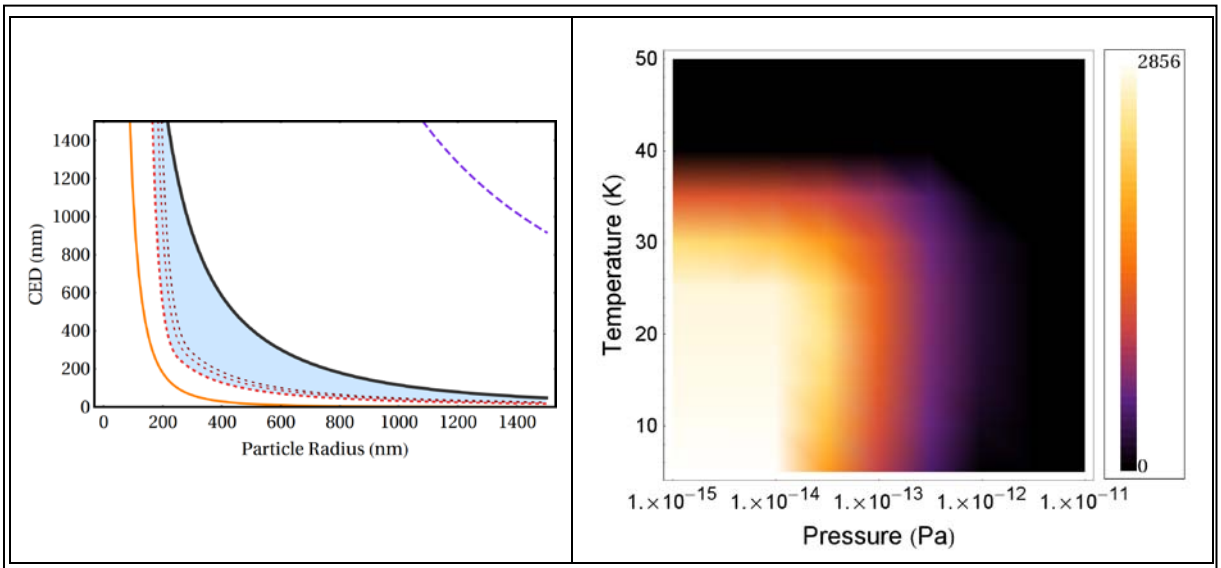

Figure 1: Coherent-Expansion Time (CED) for varying radius of the nanosphere. Here, we used the optimal parameters for the proposed experiment (32K particle and environment temperature, pressure negligible). On the right-hand side, a plot is given that indicates the size of the shaded area for differing experimental parameters (external temp. and pressure).

3.2 Scientific Requirements

In the following, we will discuss the scientific requirements for the two experiments that are

part of the proposed mission. We will also discuss in detail which of the requirements are critical for the success of the mission. It should be noted that the two experiments can be operated completely independent of each other except for the infrastructure of the spacecraft they share. This reduces the risk of a failure of the mission, and it allows, in principle, to combine any of the two experiments with other proposed missions that have common requirements in terms of orbit and stability.

3.2.1 DECIDE

In DECIDE, it will be essential to reduce any possible sources of decoherence as far as possible. Quantum superposition states are very fragile in the presence of decohering mechanisms. If a system is in a superposition of two distinct states, it essentially means that nobody could possibly know from information available in the environment of the system which state the system is in. As soon as that information leaks out from the quantum system to the environment, e.g., through collisions with other particles or other interactions, the superposition will be lost.

DECIDE Scientific Requirements on the exp. Environment and the levitated nanosphere	
Parameter	**Requirement**
Rate of collisions with gas particles	< 0.1 Hz
Temperature of the system environment	< 40K
Internal temperature of the nanosphere	< 40K
Position read-out accuracy	<1pm
Drag-free control Along cavity axis Perpendicular to cavity axis	critical <1pm over 10s <1µm over 10s
Pointing stability Cavity mirrors UV beam (relative to objective) CCD assembly IR fibers Particle loading mechanism	 Non-critical (concentric cavity) Critical (< 2×10^{-7} mrad over exp. run) < 0.1 mrad over 1s Non-critical – the cavity defines the reference mode Non-critical (only slightly reduces loading probability)
Laser stability IR laser UV laser	 1kHz line width as in LTP is more than sufficient; power stability non-critical non-critical (only very coarse power-level adjustments are necessary)
Nanosphere dielectric properties	Critical – the absorption properties have to allow for low internal particle temperatures (decoherence through the emission of blackbody radiation)
Nanosphere size	non-critical because new particles only necessary in case of rare accidental loss

Table 1: Requirements on the experimental environment and the levitated nanosphere for DECIDE. Here, we have assumed typical parameters for a double-slit experiment with HfO2 nanospheres with a radius of 220nm. The experiment in this case would typically have a duration of 10s, during which the coherence of the quantum superposition has to be maintained.

Because of this fragility, the demands on the quantum system itself and on the experimental environment are very stringent in order to prevent decoherence. For example, a single collision with a gas molecule is typically enough to decohere the quantum state. At the same time, scattering of blackbody radiation that is always present in an environment with a finite temperature, also leads to decoherence.

Requirements in order to maintain coherence over measurement time

Requirements on the environmental parameters like the density of the background gas, the temperature of the experimental system and the internal temperature of the particle are given in Table 1. These requirements are based on the consideration that quantum theory has to predict that it is still possible to observe an interference pattern after the double slit, when all relevant decoherence mechanisms are taken into account. In particular, these mechanisms are:

Requirements for the accurate measurement of interference patterns

The decoherence rates for various experimental parameters like slit spacing and observation time are determined by measuring the visibility of the interference patterns formed by the nanospheres after passing through a double-slit-type arrangement. The fringe spacing in these interference patterns is, typically, $4z_0$, where $z_0 = \sqrt{\hbar/(2m\omega_m)}$ is the ground-state extension of a mechanical resonator with mass m and resonance frequency ω_m. That means, that the fringe spacing is typically on the order of 5-10pm, and that we have to read out the position of the nanosphere with an accuracy of better than 1pm. It is possible to achieve that readout accuracy by using the cavity that is also used for trapping the particle and for preparing the quantum superposition.

Pointing stability

The most critical element in the experimental setup for DECIDE in terms of pointing stability will be the UV assembly to prepare the quantum superposition states. This assembly effectively prepares a UV beam that is focused onto spot with a radius $\leq 350\text{nm}$, and this spot has to move less than half the fringe spacing of the interference pattern to be observed, i.e., $< 2.5\text{pm}$ over the acquisition time of the complete interference pattern. This acquisition time lies between 4000s and 40000s. This extreme requirement can be relaxed if the exact position of the UV spot relative to the cavity is measured in regular intervals (e.g., before taking each data point). The detection of this relative position is TBD. Because the UV beam is focused by a reflective objective of 13mm effective focal length, the position accuracy translates into a pointing accuracy of $< 2\times10^{-7}$ mrad for the UV beam.

Since the cavity used in DECIDE is concentric, the pointing stability of the cavity mirrors is non-critical. The only translation and pointing accuracies we are sensitive to with respect to the reference system defined by the cavity are the UV beam assembly (see above), the CCD assembly, and the loading mechanism. Because we need to monitor movements of the nanospheres during their manipulation with an accuracy of at least 1µm from a distance of 5cm (distance between imaging lens and CCD), this leads to a pointing-stability requirement of 0.1mrad over the time of the manipulation sequence, i.e., 1s. The requirements on the loading mechanism are non-critical because any inaccuracies in the pointing of the mechanism only affect the probability for loading. Since loading should only be necessary before the first experiment and on the rare occasion that a particle is accidentally lost, a slight reduction in the loading probability will not affect the overall experiment performance.

Laser Stability

According to [17], ground-state cooling via side-band cooling is possible in the presence of phase-noise with a noise power spectrum $S_{\dot{\phi}}(\Omega)$ if the following condition is fulfilled:

$$S_{\dot{\phi}}(\omega_m) < \frac{g_0^2}{\Gamma_m}, \tag{0.1}$$

where $\Gamma_m = k_B T/\hbar Q$ is the thermalization rate, Q is the mechanical quality factor of the resonator, k_B is the Boltzmann constant, T is the temperature of the environment, ω_m is the frequency of the mechanical resonator, and g_0 is the single-photon coupling strength of the

mechanical resonator to the cavity mode. With the experimental parameters that we propose for DECIDE, this amounts to $S_\phi(\omega_m) < 10^{19}\,\mathrm{Hz}$, a condition that should easily be fulfilled. For comparison, one can take the results presented in [18], where a model is fitted to the phase noise measured in a laser that shows poorer performance than the narrow line-width laser used on the LTP module, which we are also proposing to use for MAQRO. The measured data in [18] agree well with the suggested model that includes white noise, flicker, and random-walk noise contributions. Using that laser, we would expect $S_\phi(\omega_m) = 10^{-8}\,Hz$, easily fulfilling the stability requirement for ground.-state cooling.

Intensity fluctuations will change the trap frequency and could thus change the interference pattern. However, the fringe spacing in the interferogram is proportional to the square root of the laser power, and to significantly change the fringe spacing, immense fluctuations would be necessary. Thus, intensity fluctuations are non-critical.

The exact power of the UV laser beam is irrelevant. It only has to be switchable between completely off, a laser power of several nW for preparing the quantum superposition by scattering, and a laser power of several mW for ejecting spurious particles from the sphere.

Drag-free control

After the nanosphere has been cooled to its ground-state of motion, it is released in order to let the wavepacket expand freely. This free expansion, which is only interrupted by the firing of the UV beam for the preparation of the macroscopic quantum superposition, typically takes place over a time of 10s. At the end of that time, the wavefunction of the particle should, according to quantum theory, have formed interference fringes with a typical spacing of 6pm. At that moment, the position of the particle is read out via the cavity. In order to be able to integrate the resulting positions from multiple such experiments over time, the position of the interference pattern with respect to the cavity has to be defined better than half the distance between two neighboring interference fringes, i.e., 3 pm. The only force acting on the spacecraft that has to be compensated is caused by the solar wind. This is on the order of several µN but has a negligible amount of noise. The drift of the particle with respect to the cavity should thus be limited by the propulsion system for drag-free control and by the sensor accuracy.

With current micro-propulsion techniques, an optimized drag-free control system, and given that the accuracy of the CASE inertial sensor should be on the order of picometers, this seems to be a feasible goal. Further studies will be required in order to find an optimized design for the drag-free control to allow for the necessary positioning accuracy of the spacecraft with respect to a free-falling test mass.

3.2.2 Critical issues

Several techniques used and requirements needed are critical for the mission and have to be further investigated in technical studies:

- **Drag-free control:** the position of the cavity with respect to the freely propagating nanosphere has to be kept stable with an accuracy of $1\mathrm{pm}/\sqrt{\mathrm{Hz}}$. Further development will be necessary.
- **Loading mechanism:** while most of the concept should work as proposed, the release of particles via ultrasonic vibrations from a glass plate has so far only been demonstrated with microspheres of several µm in diameter while the spheres used in the proposed experiments have a radius of several hundred nanometers. A solution to

overcome the stronger London van-der-Waals forces for smaller particles might be to nanostructure the surface of the storage plate to reduce these forces.

- **Ground-state cooling:** this has been demonstrated already with nanoresonators in superconducting microwave cavities, and recent progress shows much promise that this goal will soon be achieved in optical systems as well. However, so far demonstrations using levitated nanospheres are missing although experimental work is in progress and detailed theoretical studies show that the experience from other nanoresonators should be applicable for these systems as well.
- **Cavities in space:** a critical requirement of the proposed mission is the high-finesse cavity with a finesse of ~ 10000. So far, such high-finesse cavities have not been demonstrated in space missions but several proposed missions rely on this technique, and we are confident that the ongoing development effort will soon provide feasible venues for a technological realization of this central element of our experiment.
- **CCD cameras:** while CCD cameras in the IR and deep IR have been developed for various space missions, CCD cameras working in the NIR range and in the UV will TBD. In particular, the camera used will have to operate at very low temperature (30K) and under extreme vacuum conditions (interplanetary vacuum level). Recently developed CMOS cameras might provide a feasible alternative.

3.2.3 CASE

In CASE two acceleration sensors are used: The micro-sphere trap inertial sensor and the reference accelerometer. The cavity axis defines the x-axis and is aligned with the respective x-axis of the reference sensor (ONERA). The Drag-Free Attitude and Control System(DFACS) takes the input from the micro-sphere trap position sensor to control the micro-propulsion thrusters of the space-craft. As soon as the micro-sphere moves away from its nominal initial position, the DFACS commands the thrusters such that the space-craft remains centered on it. Unlike LPF, MAQRO only uses drag-free control over a single test-mass (the micro-sphere) and only one degree of freedom (the x-axis), which greatly simplifies the control and the propulsion system requirements. Note that in default operating mode the position of the second test-mass (reference sensor) does not feed-back to the DFACS but is coupled to the space-craft instead. As an alternative it is possible to couple the second test-mass to the first one, in close analogy to the "M3 mode" of LPF. A detailed analysis of the respective pros and cons of both operation modes should be covered in a dedicated study. A schematic of the MAQRO DFACS in default mode is shown in Figure 1.1 below.

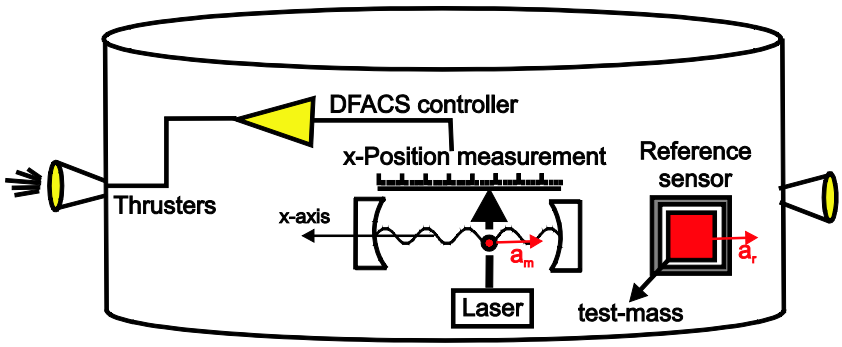

Figure 1.1: The drag-free attitude and control system of CASE. The space-craft is symbolized by the cylinder with thrusters attached to the sides.

The central science requirement for CASE is to measure the difference in acceleration (Δa_{diff}) between the microsphere (experiencing acceleration a_m) and the reference sensor (experiencing acceleration a_r) with accuracy better than $10^{-12} ms^{-2}/\sqrt{Hz}$.

Primary Science Requirement CASE	
For a Highly eccentric orbit Measure the differential acceleration between two objects of large mass difference under the influence of a large external gravity field with accuracy of better than $10^{-12} ms^{-2}/\sqrt{Hz}$. The difference between the two accelerations is the basis for determining a violation of Einstein's weak equivalence principle. The measurement accuracy should suffice to confirm/rule out several of the existing hypothesis for modifications to the standard theory. **For a L1/L2 orbit** Measure the differential acceleration between a micro-sphere and a reference sensor with accuracy better than $10^{-12} ms^{-2}/\sqrt{Hz}$. Trapping, suspension, manipulation of the sphere as well as position readout shall only use optical and not electrostatic forces.	
Secondary Science Requirement CASE (derived)	
The accuracy of a measurement of the differential acceleration Δa_{diff} between a micro-sphere and the test-mass of the reference sensor, after compensation of residual gravity gradients inside the space-craft, should be:	$LSD(\Delta a_{diff}) =$ $LSD(a_m - a_r) < 10^{-12} ms^{-2}/\sqrt{Hz}$
The accuracy of the position measurement of the microsphere should be	$< 1\text{pm}/\sqrt{\text{Hz}}$

Table 1.1: The science requirements of CASE.

One must keep in mind that the gravity gradients inside the space-craft cannot be completely nulled (e.g. for LPF there is a remaining gradient of $10^{-9} ms^{-2}$ acting on each test-mass) and that the remaining gradient is not better known than $10^{-11} ms^{-2}$ (typical error for LPF). The error on the remaining gradient is determined by the finite accuracy of the space-craft mass model which documents the exact position and mass distribution of all units and the space-craft structure

Thruster noise is fairly small for the FEEPS (Field Emission Electric Propulsion). Most of the thruster noise is removed when the two measured accelerations are subtracted from another. However, imperfect common mode cancellation sets an upper limit on the allowed thruster noise and –assuming the common mode noise rejection is identical to LPF- requires the thruster noise for MAQRO to be less than $\sim 10^{-8} ms^{-2}/\sqrt{Hz}$.

Measurement Requirement	abbreviation	Requirement value	LTP (if applicable)
1.) Experimental measurement time	T	100 s < T < 1200 s (perigee passage time for HEO)	T < 24 h
2.) Sensor accuracy microsphere	a_m	$a_m < 10^{-12} ms^{-2}/\sqrt{Hz}$ $100\,mHz < f_s < 10\,Hz$	
3.) Sensor accuracy reference sensor	a_r	$a_r < 10^{-12} ms^{-2}/\sqrt{Hz}$ $100\,mHz < f_s < 10\,Hz$	

4.) Differential acceleration measurement	Δa_{diff}	$\Delta a_{diff} < 10^{-12}\, ms^{-2}/\sqrt{Hz}$ $100\,mHz < f_s < 10\,Hz$	$\Delta a_{diff} < 3\times10^{-14}\, ms^{-2}/\sqrt{Hz}$ $3mHz < f_s < 30mHz$
5.) Thruster noise (common mode)	N_t	$N_t < 10^{-8} ms^{-2}/\sqrt{Hz}$ $10\,mHz < f_s < 10\,Hz$	$N_t < 2\times10^{-10} ms^{-2}/\sqrt{Hz}$ $10\,mHz < f_s < 10\,Hz$
6.) Uncompensated gravity gradient in experiment volume	$G_{\max}$	$G_{\max} < 10^{-9}\, ms^{-2}$	$G_{\max} < 10^{-9}\, ms^{-2}$
7.) Unknown error on residual gravity gradients	G_{err}	$G_{err} < 1\times10^{-11}\, ms^{-2}$	$G_{err} < 1\times10^{-11}\, ms^{-2}$

Table 2.1: the main measurement requirements for CASE.

Measuring the residual gravity gradients

If an acceleration measurement is performed for CASE there is a known gravity gradient offsetting both accelerations (on the order of $10^{-9} ms^{-2}$) and on top of that an unknown offset ($10^{-11} ms^{-2}$). There are two ways to overcome this problem:

1.) **Better accuracy of the gravity model than for LPF:** This should be feasible because the CASE experiment has no large floating test-masses which are in very close proximity (~2 mm) to a confining electrode cage that completely dominates the surrounding gravity gradients. The reference sensor should also be simpler and allow for a more accurate mass model.

2.) **Adjustable compensation mass inside space-craft:** When the space-craft is in drag-free motion at L1 we assume that there is no external gravity field and only internal gravity acts on the test-masses. A measurement of the acceleration is dominated by the internal space-craft gravity gradient. However, the measurement accuracy is limited to $10^{-11} ms^{-2}$, which is the uncertainty in our knowledge of the internal gradient. This makes it impossible to test the equivalence principle with a relative accuracy of $10^{-12} ms^{-2}/\sqrt{Hz}$ if only a single measurement is performed. However, if a compensation mass of 1 kg, which is located approximately 0.5 m from the test-mass, is moved by a distance of 1 cm, the gravity gradient changes by $10^{-11} ms^{-2}$. If we assume that the error of the displacement of the proof mass is as big as 1 mm (i.e. we move the mass by 9 mm instead of 10), the corresponding error just reaches our acceleration resolution limit of $10^{-12} ms^{-2}$ (and is therefore negligible). We can therefore, in a controlled way, change the proof mass in steps of 1 cm and change the overall gravity gradient in steps of $10^{-11} ms^{-2}$. For each step the accelerations can be measured and compared. This way the uncertainty of the internal gravity field ($\sim 10^{-11} ms^{-2}$) can be overcome through a series of comparative measurements. The moving compensation mass concept has the added benefit of taking a series of measurements instead of a single test at one specific gravitational environment. For this procedure to be feasible, the proof mass must be located in between the micro-sphere and the reference sensor cube, otherwise the changes to the gravity gradient induced by moving the compensation mass cancel as “common mode”, when the two accelerations are subtracted. Alternatively, a compensation mass of 2 kg could form an equilateral triangle of 0.5 m side-length with the micro-sphere and the reference sensor. The compensation mass could then be fixed to the optical bench support structure in the space-craft inner cylinder on top of the bench and the reference sensor.

Highly elliptical orbit for CASE

The experiments for CASE would ideally be performed in a highly elliptical orbit which takes the space-craft close to earth so that the test-masses experience a large gravity gradient. At a HEO of (650 000 km apogee height / 3800 km perigee height / total orbit period ~ 22 days), the gravity gradient at the perigee is ~0.4 g ($g \sim 10 ms^{-2}$) and which allows us to perform a measurement of the gravitational acceleration with a fractional accuracy of $10^{-12} ms^{-2} / 0.4 ms^{-2} / \sqrt{Hz} = 2.5 \times 10^{-12} \sqrt{Hz}$. The time spent at the perigee (space-craft within 3800 km-4500 km height) is 20.2 minutes, which is sufficient to perform the acceleration measurements necessary to test the equivalence principle. Longer experimental times come at the expense of reduced fractional accuracy. An optimized balance between dynamic factor and measurement time requires a more detailed analysis. Calibration of the residual gravity gradients, along the lines described above, could be performed during the two weeks while the space-craft is at the apogee, together with the DECIDE experiments. At the apogee of the highly eccentric orbit, at a distance of close to 700 000 km from earth, there are similar experimental conditions to the ones at L1/L2. The experimental measurement time there is much longer than at the perigee, on the order of ~2 weeks. All experiments for CASE and DECIDE, including calibration and preparatory experiments, could be performed during 6 months of operation, which amounts to 8 orbital periods.

4 Mission profile proposed to achieve these objectives

The science requirements indicate that an extremely good vacuum, very low temperatures and experimental measurement times of several seconds are required for DECIDE. On the other hand, CASE requires a medium-quality vacuum, room temperature and very long experimental measurement times combined with very good temperature stability and minimal drag-forces. A mission to L1/L2 is ideally suited and fulfils the respective requirements for both experiments.

4.1 Orbit requirement

Follow Pathfinder's example, the MAQRO space-craft is injected into a halo orbit round the sun/earth Lagrange point L1 (L2 would be a feasible alternative), following the initial injection into elliptical earth orbit and 8 apogee raising orbits.

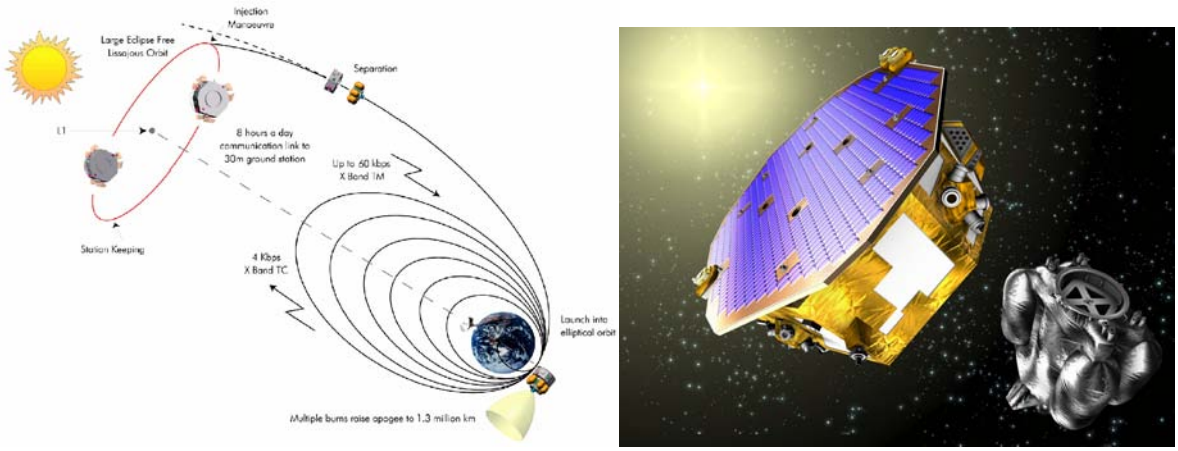

Figure 1.1.: The LISA Pathfinder orbit is also chosen for MAQRO. The Pathfinder space Science module is separated from the Propulsion Module (artistic graphics, ESA).

The spacecraft is injected into a low orbit by the Launch Vehicle. Separation from the upper stage may occur in sunlight or eclipse. Following separation the Chemical Propulsion Subsystem will initialises, following an initialisation sequence controlled by On Board Software (OBSW). During this period, which may partly be in eclipse, there is no attitude control, and the spacecraft tumbles uncontrolled, with power mainly or solely from the battery (a 600 Wh battery fulfils the needs of MAQRO). Once sensors and actuators are available, a transition to Sun Acquisition mode is autonomously performed.

Shortly before reaching the final on-station orbit around L1, the Propulsion Module (PRM) is separated from the Science Module (SCM). After separation, the spacecraft is spin-stabilised sun pointing. The nominal attitude profile is maintained using the micropropulsion subsystems. In contrast to LISA Pathfinder, MAQRO will only use Caesium-slit FEEP thrusters (providing $0.3\,\mu N - 100\,\mu N$ variable thrust, specified for >2000 Ns firing) and not additional colloidal thrusters of the disturbance reduction system (DRS), which shall be removed. Asides from a considerable simplification, this effectively decreases the space-craft mass by ~37 kg.

4.2 Alternative orbits

It is alternatively possible to take the mission to a highly eccentric earth orbit instead of L1/L2 and still fulfil the science requirements of DECIDE and CASE. Considering an ellipse of (0.7 million km / 4000 km) the orbital period would be ~ 3 weeks, from which ~ 2 weeks are spent around the outer extremum, which is suitable for science experiments. It is possible to compress the experimental schedule for MAQRO and fit all experiments into only 2-3 orbits. The impact of heavy radiation doses when crossing the Van-Allen belt and large thermal gradients and strains when approaching earth must be discussed in detail before a proper judgment can be made.

It is even conceivable that a low-earth orbit could be another viable alternative. Further investigations must determine if a different heat shield design allows to effectively shield DECIDE against the sun as well as the earth and if the stringent vacuum requirements can be met in the experimental volume located in the wake of the shield. More analysis on the mission-critical temperature and its stability as well as the achievable vacuum levels of a re-designed space-craft and heat-shield would be required to investigate this alternative.

4.3 Mission lifetime

The total mission time will be 6 months. Multiple burns (9 for Vega and 15 for Rockot) raise the apogee to 1.3 million kilometres during 15 days. The following transfer to L1 (1.5 million kilometres from earth) takes 30 days. After science payload commissioning (including an optional bake-out) the science experiments are scheduled for another 4 months, raising the total to ~ 6 months.

4.4 Communication, mass data storage, ground segment assumptions

A communication window of 8 hours per day, as in the Pathfinder mission, is sufficient to transfer science data to ground. Data are received by the 35 m Cerebros antenna and transferred to ESOC for further processing. Considering a maximal rate of 20 kbit/s of science and attitude control data during experimental runs, the data recorded during 24 hours of science runs can be transferred to ground at 60 kbit/s in the 8 hour communication window

each day. The on-board computer architecture should provide the means to continuously store science data for a period of up to three days in a solid state mass memory (SSMM), which implies a minimal capacity of ~650 Mbytes, which is easily achieved with any modern mass memory (capacity up to 2 TeraBit).

A brief overview over the main requirements for the mission profile is given in table 3.1 below

Mission requirement for	Suggested solution	Alternative solution
Launcher	Vega	Rockot
Space-craft platform	Pathfinder platform with science spacecraft and propulsion module	Split DECIDE from CASE and include either experiment with other science experiments on separate mission.
Preferred orbit	Halo orbit around L1 (alternatively L2)	Highly eccentric earth orbit (HEO) of 7E5 km / 35E3 km
Mission lifetime	6 months	Extension periods of 6 months for L1 Mission lifetime of ~2-3 months for HEO
Communication	60 kbps TM, 2 kbps TC, communication for 8 hrs/day	Lower BW: 30 kbps TM, 1 kbps TC smaller antenna/
Mass data storage on-board	Solid State Mass Memory (SSMM) of 1 GigaByte	OBC on-board memory for science data storage of >250 MBytes
Ground segment assumptions	Cerebros, Spain (35 m)	Using smaller antenna possible for larger transponder power (>6 W) and / or lower communication BW

Table 3.1: Main Mission requirements

4.4.1 DECIDE

The data taken in this experiment will be a series of data points, each of them representing the position where a nanosphere has been detected along the cavity mode. The overall collection of these data points then comprises an interferogram that represents the result of one experimental run. Each position has to be measured with an accuracy of $\sim 10^{-13}\,\mathrm{m}$ and thus is best represented by a double precision floating-point number (64 bits or 8 bytes).
The experimental procedure in order to successfully load nanospheres into the cavity is $\sim 150\mathrm{s}$. This only has to be performed before the first experiment, and later on in the event that a particle is lost from the cavity field, which should according to our estimates never happen. Thus, this time should not have to be included in the average time it takes to perform an experiment and in the corresponding stability considerations. If a particle is lost, the experiment should be aborted until a new particle has been loaded by repeating the loading procedure.
Once one or more than one particle is in the trap, an automated procedure will manipulate the particles to make sure that one and only one particle remains in the cavity and that this particle is moved to the experimental region where the UV beam intersects the cavity mode. This process takes $\sim (N+2)$ seconds, where N is the number of particles that have originally

been loaded into the cavity. Here, we assumed 1 second to manipulate and eject each of the spurious particles and 1 second each for feedback cooling in the beginning and the end of the manipulation procedure. The cooling into the ground state via side-band cooling takes about 200µs. From that moment on it typically takes 10 seconds to prepare the quantum state and propagate the nanosphere. That means, the overall process as soon as we have only one particle in the cavity takes about 13 seconds (we neglected the 200µs it takes for ground-state cooling).
If we add 1s cavity readout time and a success probability of $1/3$ for the preparation of the quantum superposition, the average overall time for one run of the experiment is $13\times 3+1=40$ seconds until we have successfully detected the position of a particle after the propagation through a double slit. See the flow diagram of the overall experimental flow.
Every time the preparation does not succeed as well as at the end of a successful experiment, the trapping beam is switched on and the CCD checks whether the particle is still trapped. If it is, we start the manipulation and cooling circuit again. Only in the unlikely event that the particle is lost during an experiment, will the loading mechanism be used again.
The typical fringe spacing in the measured interferogram is 5pm, and the interferogram will have a FWHM of 2µm. That means that the measured positions of the nanosphere will be spread over 4×10^4 fringes. Given that it takes 40s to prepare and measure one point of the interferogram, it is unfeasible to resolve the full pattern. However, since the resolution of the positon measurements is higher then the fringe spacing, we only need enough points to make a statistically significant judgment for a lower bound on the visibility of the interference pattern. Given between 100 and 1000 data points should provide the necessary information but a detailed study of the ideal statistical methods for data analysis will be necessary.
Assuming between 100 and 1000 runs for one interferogram, the overall acquisition time for one experiment is between 4000s (1.1h) and 40000s (11h).

4.4.2 Communication and ground-segment requirements

A communication window of 8 hours per day, as in the Pathfinder mission, is sufficient to transfer science data to ground. Data are received by the 35 m Cerebros antenna and transferred to ESOC for further processing. Considering a maximal rate of 20 kbit/s of science and attitude control data during experimental runs, the data recorded during 24 hours of science runs can be transferred to ground at 60 kbit/s in the 8 hour communication window each day. The on-board computer architecture should provide the means to continuously store science data for a period of up to three days in a solid state mass memory (SSMM), which implies a minimal capacity of ~650 Mbytes, which is easily achieved with any modern mass memory (capacity up to 2 TeraBit).Proposed model payload to achieve the science objectives

5 Proposed model payload to achieve the science objectives

5.1 Overview over all elements

The MAQRO mission comprises two independent experiments named

- DECIDE (Decoherence In a Double-slit Experiment)
- CASE (Comparative Acceleration Sensing Experiment).

Although the two experiments cannot be cleanly split into two instruments (they share the laser and data-management unit), an alternative cold redundancy concept would provide a

separate laser and DMU for each experiment and therefore define two separate instruments.

The experiments comprise the following subsystems and units:

Experiment	subsystem	component
DECIDE	Micro-sphere trap	Optical Bench (exterior)
		CCD chip & electronics
		IR Laser Assembly
		UV Laser Assembly
		Cryo-Harness
	Thermal control subsystem	Heat shields and struts
		Launch lock mechanism /
	Data-Management Unit	Processor
		Software
CASE	Micro-sphere accelerometer	Optical Bench (interior)
		Phase-meter
		IR Laser Assembly
		Phase-meter
		Venting ducts
	Gravitational reference sensor	Sensor Unit (SU)
		Interface & Control Unit (ICU)
	Data-Management Unit	Processor
		Software

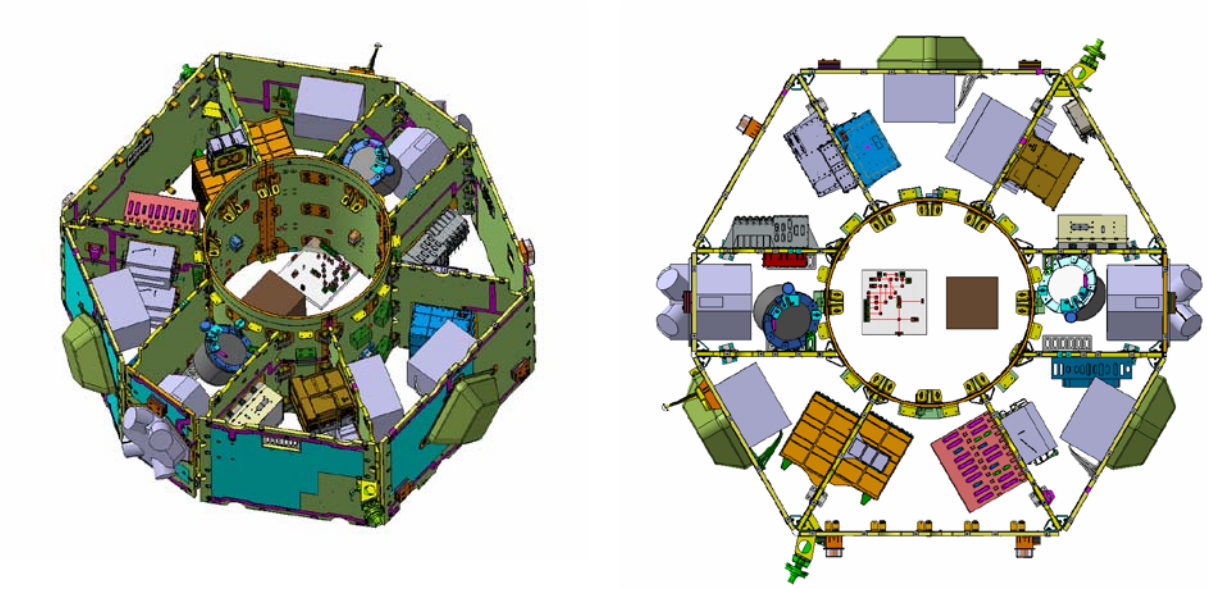

Figure 5.1: 3-d illustration of the LPF Platform with modifications for MAQRO. The picture shows the LPF Platform with all the units (payload units and science-space-craft units) that are typically used on LPF. Some modifications as they are proposed for MAQRO are illustrated: in the inner cylinder one can see the optical bench for CASE and a cube indicating the ONERA sensor (200 mm x 200 mm x 200 mm).

5.2 The Optical Bench of DECIDE

Figure 5.2 shows a top-down view of the optical bench (20x20cm) for DECIDE, which is

attached outside of the spacecraft as is illustrated in the description of the thermal shield in section 6. Figure 5.2 shows a corresponding 3D illustration of the setup where it is possible to see the three struts that connect the setup to the spacecraft inner cylinder.

A detailed description of the steps taken in a typical experiment is given in section 5.4.´The central elements of the experimental setup as illustrated are the following:

- A cavity with finesse ~ 10000 for trapping, cooling, manipulating and high-precision position readout of dielectric nanospheres. The mirrors are assumed to be separated by 10cm, and the mirrors to each have a curvature radius of 5cm and reflectivities of 99.95% and 99.99% for the input and end mirror, respectively. The beam waist within the cavity is $10\,\mu\mathrm{m}$.

- A high-numerical-aperture reflective objective for focusing a UV beam for particle manipulation. Its effective focal length is 13mm, the numerical aperture is 0.4, and the working distance is 24mm.

- Polarization optics to separate the beam reflected from the cavity (for signal readout and Pound-Drever-Hall (PDH) cavity locking), which will be vertically polarized, from the input laser beam, which will be horizontally polarized. While only one beam is depicted, there are actually two frequency-shifted beams sharing the mode. One beam is on resonance with the cavity to trap the particle, the second beam is detuned and is used to side-band cool the particle's center-of-mass motion as well as to read out its position after each experimental run. The trapping beam will be modulated via an acousto-optic modulator (AOM) to facilitate PDH locking, and the second beam will be offset in frequency by using an electro-optic modulator. These elements are placed on the laser module within the spacecraft (not shown). The laser beams are directed onto the exterior platform via single-mode fibers that are mounted in single-mode fiber couplers akin to the ones used in LTP and bonded to the optical bench for maximal pointing accuracy.

- A CCD camera (or alternatively a CMOS camera) for the observation of UV light scattered from trapped particles and for detecting particle positions for calibration purposes, and for the controlled manipulation of particle positions. While the camera only needs reasonable efficiency in the NIR range in order to detect particle positions, the efficiency in the UV range should be as high as possible because the efficiency with which scattered UV photons are detected will enter the visibility of the observed interference pattern. A UV lens (not shown) with a focal length of 5cm is used to image the experimental region onto the camera. The position of the camera in the figures is meant to be illustrative but in the actual setup the camera should be mounted such that the UV beam does not hit it. A possible position would be above the reflective objective and angled down toward the experimental region.

- UV single-mode fiber coupler. Similar to the NIR single-mode fiber couplers, this coupler will be used to collimate the UV laser beam supplied through a single-mode fiber that is connected to a low power (~10mW) UV laser within the spacecraft.

- A nano-particle loading mechanism is mounted below the optical bench to load the cavity with nanospheres whenever needed. This loading mechanism is described in detail in section 5.4.

- A quadrant-diode (not shown) to measure NIR light scattered from the trapped particle and a lens with a focal length of 3-5 cm to image the light onto the diode.

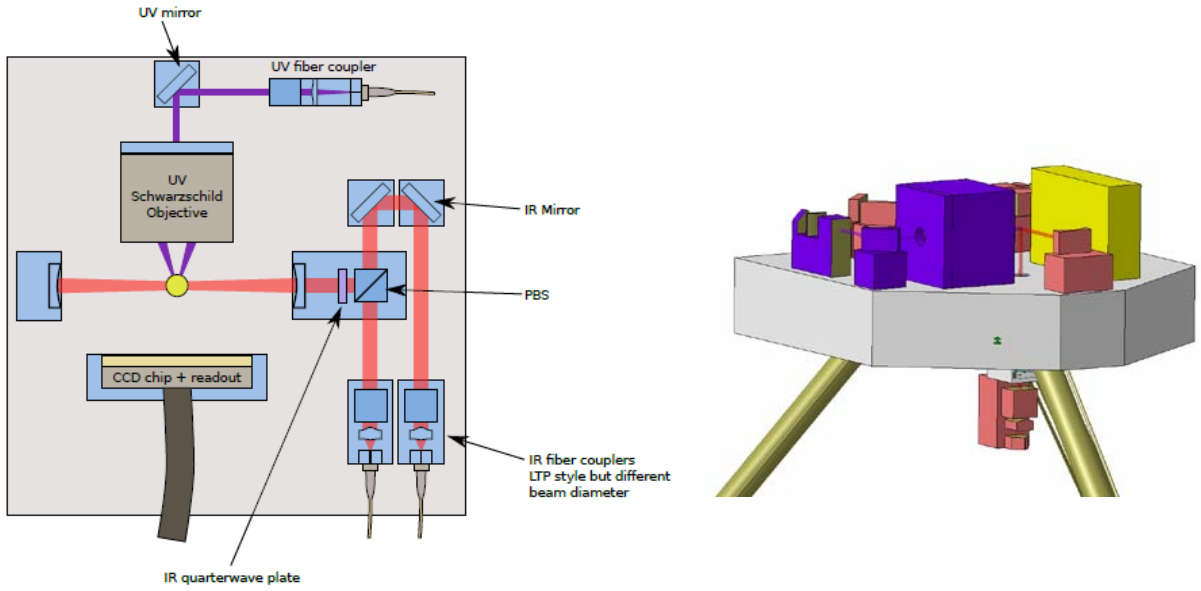

Figure 5.2: (left) Top-down view of the DECIDE optical bench, (right) 3-d model of the DECIDE optical bench.

5.3 The optical bench of CASE

A top-down view of the optical bench of CASE is given in Figure 5.3 below. Figure 5.4 show corresponding 3-d illustrations. The dimensions of the optical bench are 25x25cm, and a grid with a spacing of 1cm is laid over the bench to give an impression of the dimensions and positions of the various components.

Essentially, the setup consists of two parts (a detailed description of the elements is given below):

- An interferometric setup for laser stabilization that is modelled on the setup designed for LTP.
- A setup to trap a microsphere and to measure its position relative to the optical bench.

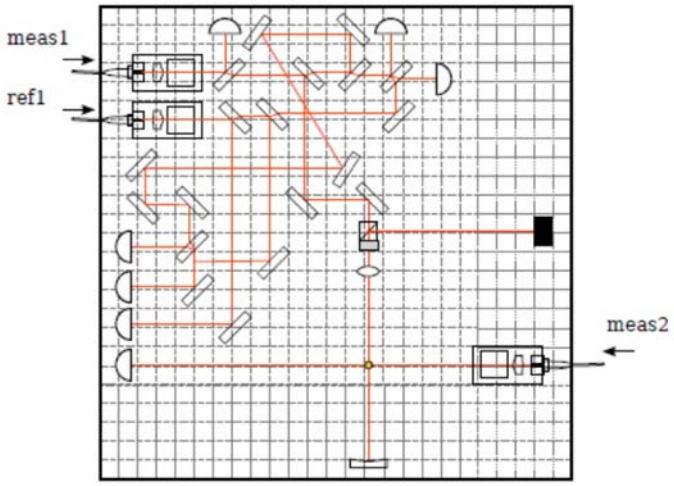

Figure 5.3: Top-down view onto the CASE optical bench.

A 3-d model of the CASE optical bench is given in Figure 5.4 below:

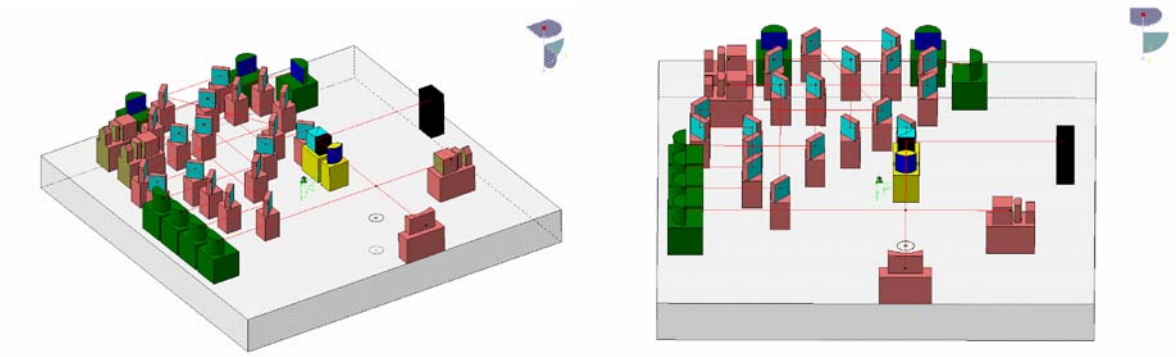

Figure 5.4: 3-d model of the CASE optical bench.

The interferometric setup uses two beams that are frequency shifted by ~1.6kHz with respect to each other in order to allow for the heterodyne detection of phase shifts. Both beams are directed onto the platform via single-mode fiber couplers that are bonded to the optical bench for maximum beam-pointing stability. This part of the setup consists of two interferometers. In one of them, the path lengths are balanced whereas in the other the path lengths are intentionally unbalanced in order to facilitate the observation (and the stabilization) of laser phase drifts. Each of the two interferometers uses two split photo diodes for heterodyne detection. In addition, a part of each beam is split off and its power monitored via an additional photo diode for each beam in order to provide a feed-back signal in order to detect and stabilize against power fluctuations of the laser.

In order to trap the microsphere used for inertial measurements, part of the beam denoted by “meas1” is sent through a quarter-wave plate and a polarizing beam splitter. It is then focused via a lens with a focal length of 5cm and then reflected back onto itself via a spherical mirror with a focal length that is slightly shorter than 5cm in order to allow for stable trapping of the microsphere. The position of the sphere (in principle, in all spatial directions) is measured by scattering an additional laser beam off the sphere and measuring the interference pattern that is formed between the scattered and unscattered light. This beam is slightly focused to a waist that is about twice the size of the trapped sphere. If necessary, the position signal can also be used for feed-back cooling of the center-of-mass motion of the sphere.

5.4 Operations and measurement technique

The overall flow of operations for DECIDE is described in the experiment flow chart.

5.4.1 Loading mechanism for optical levitation (CASE and DECIDE)

The loading mechanism for nanospheres (DECIDE) and for microspheres (CASE) can be built along the same principles. In the following, we will discuss the working of the loading mechanism in detail for DECIDE. For CASE, the same mechanism can be adapted by accordingly increasing the power of the acceleration beam, the time for which it is switched on, and its waist size. This is TBD but should pose no principle limitations since the manipulation of microspheres with a radius of 150µm is significantly easier than the manipulation of nanoparticles and could, in principle, even done via mechanical transportation. For example, the manipulation which will be described below to ensure that only one nanosphere is loaded in the cavity, is simpler for large spheres because it is straight-forward to launch single spheres from an array of piezo-electric elements that can be manufactured with a size comparable to the sphere itself.

The mechanism for loading nanospheres comprises three distinct steps (experiment flow

chart):

- Particles that are deposited on a glass surface are shaken loose via ultrasonic vibrations caused by a high-frequency piezo actuator, which is switched on for several microseconds.
- About 100s after the Piezo stops, a 10mW IR laser beam with a waist of 41μm is switched on for 79μs and passes by the surface of the glass plate in a distance of $\Delta x = 5\text{mm}$. It collects any spheres that were freed with an average velocity of $(5.0 \pm 0.2) \times 10^{-5}\,\text{m/s}$ perpendicular to the glass plate. These spheres are accelerated by the radiation pressure of the laser beam to transport velocity of 1.2 mm/s.
- The nanospheres travel from below through a hole in the base plate over a distance of $\sim 62.5\text{mm}$ to a position 25mm above the base plate. This takes $\sim 52.1\text{s}$. After that time, the trapping field in the cavity is switched on. At that point in time, none or several particles might be trapped in the cavity beam – the loading procedure continues with the procedure described in the next subsection.

Using these design parameters, we expect a single loading run as described above to take 152.1 seconds. In the following steps, which are described in the next subsection, an automated procedure will determined whether there has been at least one particle loaded into the cavity. If not, then the procedure above will be repeated until it succeeds. The rate of success will depend on the mechanism for freeing nanospheres from the glass plate (see below). If more than one particle has been loaded, spurious particles can be ejected via a mechanism described below.

The ultrasonic vibrations used to emit nanospheres from the glass surface are provided by a piezoelectric element (PE). The accelerations provided by the PE can reach up to 100.000 m/s^2. The forces acting on the particles on a flat surface need to overcome the London – van der Waals forces (F_{vdW}) binding them:

$$m_{sphere} * a_{piezo} > F_{vdW} = \frac{A * d}{12 z_0^{\,2}} \tag{5.1}$$

The latter expression is valid for a sphere of diameter d close to a flat surface, where A is the Hamaker constant(A=6.6 for fused silica) constant, d is the sphere diameter and z_0 the distance between the surfaces, which is typically taken to be 0.4 nm for direct contact (as the van-der-Waals force diverges for d=0) [19,20] . With this we get a necessary acceleration of:

$$a_{piezo} > \frac{\mathrm{A}}{2 d^2 \pi \rho z_0^{\,2}} \tag{5.2}$$

With the given limitation on Piezo-accelerations this mechanism can provide particles down to a size of d=3μm. This has been demonstrated experimentally in [21]. In order to reach smaller particle sizes down to several hundred nanometers, it is intended to reduce the surface forces by using a nanostructured material, which will be a matter of further technology development.

Because a particle, once it has been loaded, can in principle be used for an arbitrary number of experiments, the time needed for loading is not critical. However, in order for the loading times not to become indefinitely long, it will be advantageous to achieve a high enough success probability per trial; ideally above 50%. This will mostly depend on the velocity distribution of the nanospheres as they are freed from the glass plate and will be a matter of future investigation.

5.4.2 Automated preparation of single nanospheres

After the loading procedure into the optical cavity for DECIDE has been completed,

depending on the velocity distribution of the nanospheres freed from the glass plate (see above), there can be anything between zero or several nanospheres in the cavity. How many particles there are, can be determined automatically by monitoring the scattered light imaged onto the CCD camera. Assuming a distance of 5cm between the imaging lens (focal length: 5cm) and the CCD with a pixel size of about 10μm, let us assume that we can resolve a spot size of about 6μm in the trap. Given the size of the loading region of 1mm, the probability to load more than one particle into a region we cannot resolve, is negligibly small.

Thus, if there is exactly one scattering center with a defined brightness in the cavity mode, we can be sure that exactly one nanosphere has been loaded, and we can continue with the next step in the experimental procedure. If there is no scattering center, we will have to repeat the loading mechanism, and if there is more than one scattering center, we can proceed with the automated manipulation of the loaded nanospheres as is described in the following.

In the following steps it will be ensured that only one single particle is loaded, by ejecting the others deterministically. Further, that particle will be positioned. . Initially, the particle will be cooled by feedback cooling radially and sideband cooling longitudinally close to the ground state (final particle velocity v<3µm/s) within 1 s. An automated procedure chooses uses the CCD-image to determine the particle positions and choose a first particle for ejection The aim is then to move that particle to that experimental region and eject it via radiation pressure from the UV beam, which is ramped up to 1-10 mW for that purpose. The positioning of a nanosphere is achieved in a stepwise procedure, where we use the slope of the quantum control mode, which is phase shifted with respect to the trapping mode, in order to move the nanosphere via momentum kicks. Each step takes 260 µs (see Fig. XX). Initially, the stepping sequence is initiated, and the movement of the particle is observed over 3 frames of the CCD camera – that corresponds to 11 steps in the standing wave, which is easily resolved by the camera. This way, the algorithm finds the direction the particle moves and can then continue or change the direction (turn-around sequence). By performing step after step, the particle can be moved over a distance of 1mm (the size of the loading region) in a time <1s. Thus, the particle cannot be lost radially within that time. A prerequisite to achieve that speed is that the frame rate of the CCD camera is at least 1kHz. If the camera is slower, the procedure will be delayed by a corresponding amount.

Once the last particle is moved to the experimental region, the UV beam can be ramped down to the level of 1-10 nW. This way, it will not eject the remaining particle, but we will be able to see the scattered light in order to determine when the nanosphere has reached the experimental region. The overall process should take at maximum N seconds, where N is the number of particles initially loaded into the cavity. This should usually be on the order of 1s.

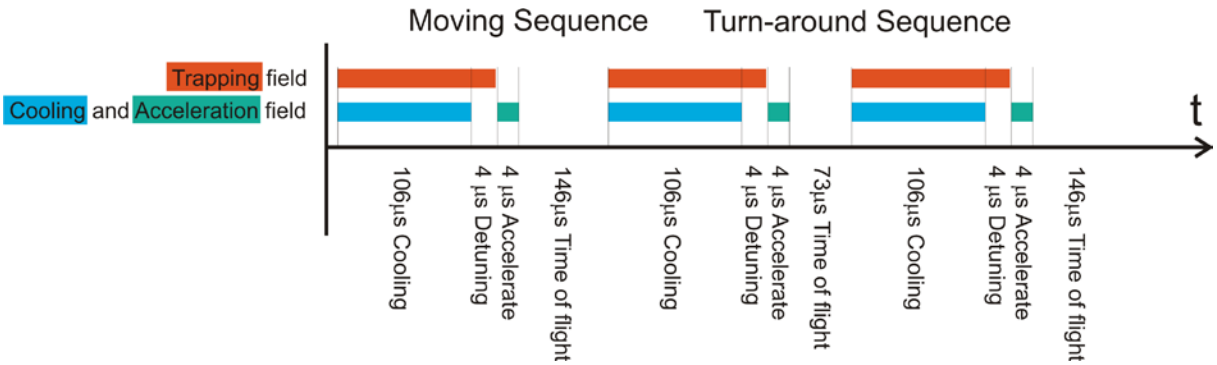

Figure 5.5: Manipulation sequence for moving the nanospheres along the cavity beam. . The longitudinal motion of the nanosphere is cooled close to the ground state via the blue-detuned quantum mode, while the particle is stored in the trap. The quantum mode laser is set to 0

detuning offline. Then the trapping mode is switched of. A momentum kick is given to the particle by switching on the quantum mode (which is set to have a l/4 shifted potential minimum). The particle moves at a speed of 7.3mm/s by 1 micrometer until where the trapping beam is switched on again after 146 μs to trap the nanosphere. A cooling sequence reinitializes the particle to the ground state. This way imprecision in the timing sequence are reset. In order to turn the particle motion around, the trapping and cooling in one sequence is reactivated after 73 μs, leaving the particle in a trap with an inverted quantum mode slope, which will excert a momentum kick in the other direction.

5.4.3 Preparation of the ground-state of motion

Once the single remaining nanosphere has reached the experimental region, feed-back cooling (for the vibrational modes perpendicular to the cavity mode) and side-band cooling along the cavity mode will be used to cool the center-of-mass motion in all three dimensions to an occupation number as low as possible. The occupation number of the transverse center-of-mass motion should be cooled down to an occupation number of approx. 10 quanta. Once this has been achieved, the cooling beam travelling along the cavity mode, will be used for side-band cooling in order to prepare the nanosphere in the ground-state of motion.

The cooling rate for side-band cooling is $\sim 18\text{kHz}$, which corresponds to an exponential decay of the occupation number with that rate. This should result in achieving the ground-state within a time <200 μs. The cooling rate of the feedback cooling is classically calculated to be approx. 250 Hz, and the maximally allowed velocity of 4μm/s is achieved after <1s.

5.4.4 Preparation of a macroscopic quantum superposition

As soon as the ground state has been reached, the cooling and the trapping beam in the cavity will be switched off. Then the wavepacket of the nanosphere will be allowed to spread for several seconds (depending on the size of the particular nanosphere and the width of the double slit we intend to prepare), and then the UV laser is ramped up to produced a short pulse of 1ns with a power of 10nW. This ensures that in a distance two waist sizes away from the beam center on average less than one photon is present in the beam while approximately 2000 photons will be present at the center. If no UV photon is scattered, we will have prepared a macroscopic superposition of the nanosphere being either on one or the other side of the path of the UV beam. This part of the preparation only takes as long as it takes to process one frame of the CCD camera – as above, we will assume a CCD frame rate of 10kHz, leading to a preparation time of the quantum superposition of $100\mu\text{s}$ if successful. The probability of success is $\sim 1/3$, which is the probability for the nanosphere to be further away from the center of the wavepacket than 1 sigma. If the particle is too close to the center, it will scatter a significant amount of UV photons, which should lead to a signal on the CCD camera – in that case, the loading procedure and preparation has to be repeated. . In that case the experiment has to start over again. The trapping beam is switched on and it is determined if the particle is still trapped. If no external disturbing event occurs this will be the case.Then the measurement sequence starts over by cooling the particle. In case the particle is lost, the loading sequence is reinitiated. However, if no UV emission is detected, the particle is assumed to have passed the double slit and the macroscopic superposition has successfully been prepared.

If the preparation has been successful, the wavepacket is again allowed to propagate for several seconds, typically the same amount of time that one let the wavepacket expand from

the ground state. Then the cavity field is turned on with low power (several mW intracavity power, i.e., about 1nW extracavity power) in order to read out the position of the nanosphere. This completes the experimental run.

5.4.5 Free propagation and measurement of the interference pattern

In order to study the decoherence mechanisms as described in section 3.1.2, the wavepacket of the macroscopic quantum superposition is again allowed to propagate for several seconds. This will typically be the same amount of time that one let the wavepacket expand from the ground state. The probability distribution of the positions where the particle is detected provides the experimental data for the decoherence test. For standard quantum theory, a interference pattern of 5 pm fringe spacing is expected.

The position detection is conducted via the cavity readout. In order to determine the position with a resolution of <1 pmwithin 1ms detection time, the quantum mode is driven with 10 pW, assuming shot noise limited phase readout of the quantum mode. After that time the trapping beam is switched back on and the measurement sequence is reinitiated (for an overview of the sequence, refer to to flowchart).

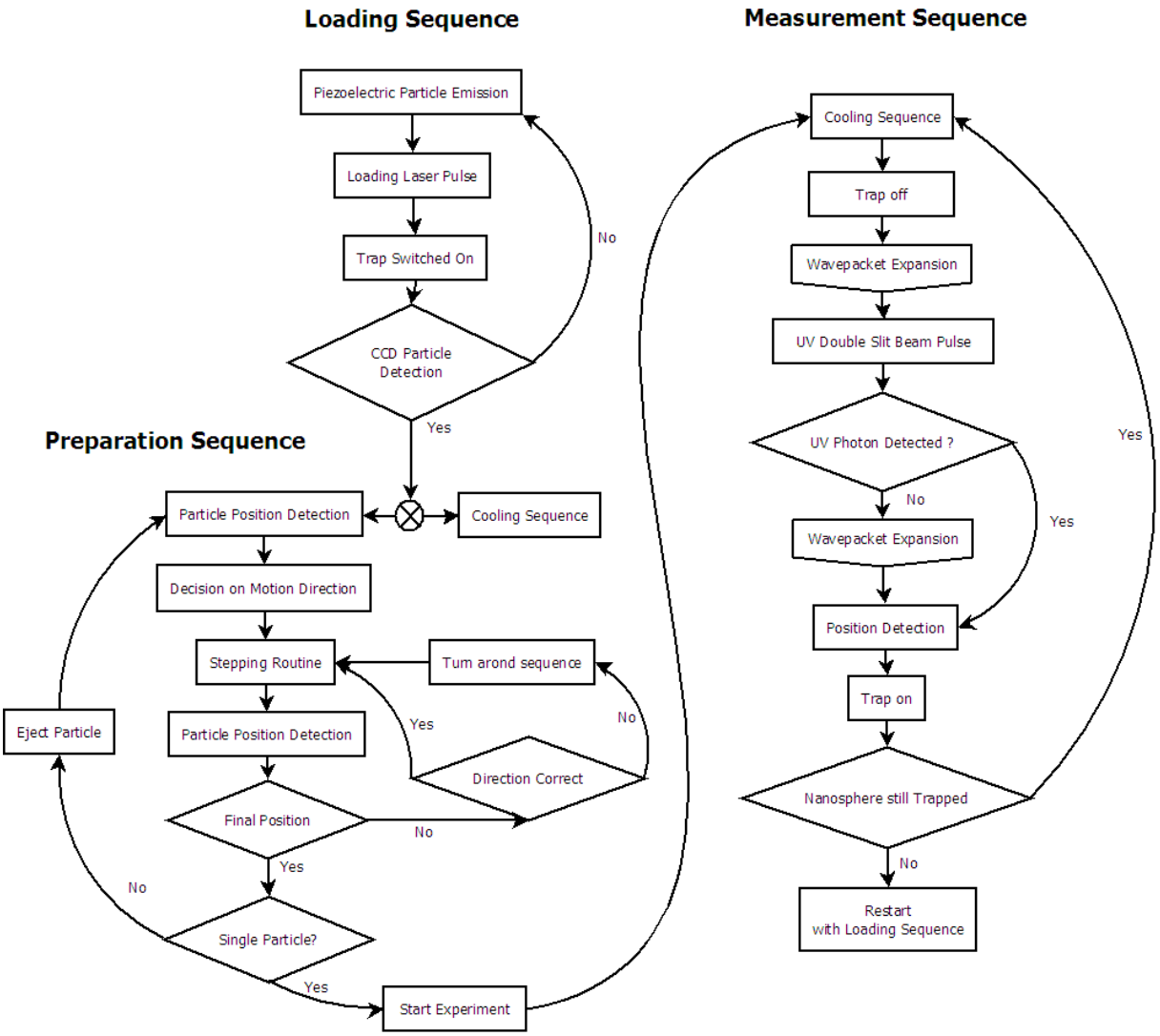

Flowchart of the particle loading, preparation and measurement sequences for DECIDE as described in detail in the text.

6 System requirements and spacecraft key issues

6.1 Payload Mass budget

The MAQRO mass budget is closely based upon the one of Pathfinder. As the space-craft platform of MAQRO is identical to the one of LISA Pathfinder, we shall focus on the MAQRO payload and compare it to LTP, the LISA Pathfinder payload. Note that in Pathfinder the payload module and service module are combined in the "Science Module". The latter is attached to the propulsion module which is ejected after reaching the final orbit at L1. The various LTP units and their respective masses are listed on the left side of table 6.1, the corresponding (if applicable) MAQRO units are listed on the right side. Those LTP units that shall be used on MAQRO as well (albeit in modified form) are assumed to be identical in weight.

It is apparent that by omitting the heavy inertial sensor from LTP the payload mass of MAQRO is dramatically reduced. For the ONERA accelerometer we used mass values similar to the ones printed in another proposal [22] and used in the GOCE mission. The UV laser assembly was assumed to be similar in mass to the IR laser assembly without modulators although this is probably completely over-estimated due to the low required UV-power (<10 mW). The heat shield and external optical bench only add ~ 20 kg to the total payload mass.

If "venting to space" [23] is implemented to achieve a good interior vacuum, the use of venting ducts slightly increases the space-craft mass. In the comparison below the venting tubes are included with the payload units because there is no dedicated section for discussing the space-craft. The mass estimate is based on two aluminium venting tubes of 10 cm diameter, 1.6 mm wall thickness and 1 m length each.

To obtain the dry total mass of the space-craft we add the mass of the science space-craft and of the propulsion module to the payload mass. Note that the weight of the science spacecraft for MAQRO is considerably reduced (by 37 kg) with respect to LPF because the disturbance reduction system (DRS) has been removed. We conservatively add the same amount of propellant as for the heavier Pathfinder space-craft. Launch adapter and weight are identical to Pathfinder and therefore the net total launch mass is also lower by ~34 kg (with optional heaters ~24 kg) than the Pathfinder launch mass, including rather generous margins.

Launch Composite	LPF Mass (kg)	CBE MAQRO Mass (kg)	Maturity margin	CBE +Margin
Payload /LTP	144	96(+7)	30%	124(+10)
Science Space-craft (w.o. LTP)	274	237	5%	249
Propulsion Module	210	210	5%	221
Launch composite dry total	628	543 (+7)		594 (+10)
Consumables	1110	1110		110
Launch composite wet total	1738	1653 (+7)		1704(+10)

Table 6.1: the total mass budget for MAQRO (third column) compared to the total mass budget of Pathfinder (second column). Optional equipment is listed in brackets.

Items & units LTP	Mass (kg)	Items & units MAQRO	Mass (kg) CBE	Maturity margin	CBE+Margin
Inertial sensor head	40	Accelerometer sensor Unit	11	5%	11.6
Inertial sensor FEE	32	Accelerometer Control Unit	4	5%	4.2
Caging mech. control unit Charge management dev.	11	Heat shield (incl. struts, inserts and launch locks, protective cover and margin)	10	50%	15.0
		Optional: Shield extension: mechanism Shield baking: heater + power unit	 (2) (5)	50% 50% 50%	 (3.0) (7.5)
		Optical bench (exterior)	3	30%	3.9
		CCD readout electronics	2	100%	4.0
Optical bench assembly (interior)	17	Optical bench assembly (interior)	14	60%	22.0
Optical Bench & components	4	Optical Bench & components	4	25%	5.0
Sideslabs	9	Support Structure	6	50%	9.0
Other	4	Other	3	100%	6.0
		Particle dispensers (interior + exterior)	1	100%	2.0
		Venting to ducts to space	3	20%	3.6
Laser Assembly (IR)	9	Laser Assembly (IR)	9	10%	9.9
Power & Control Unit	4	Power & Control Unit	4	10%	4.4
Laser Modulator	4	Laser Modulator	4	10%	4.4
Laser Unit	1	Laser Unit	1	10%	1.1
		Laser Assembly (UV)	5	60%	8.0
		Power & Control Unit	4	50%	6.0
		Laser Unit	1	100%	2.0
Phase-meter	4	Phase-meter	4	25%	5.0
Payload processor (DMU)	8	Payload processor (DMU)	8	10%	8.8
Diagnostic elements (sensors,…)	3	Diagnostic elements (sensors,…)	3	20%	3.6
Assembly & interface equipment	7	Assembly & interface equipment	7	20%	8.4
Harness	13	Harness	13	20%	15.6
Total	**144**	**Total**	**96+(7)**	**average: 30%**	**123.6+(10.5)**

Table 6.2: The MAQRO payload mass budget compared to the LTP mass budget.

6.2 Power budget

In table 6.3 the power budget of the MAQRO payload is compared to LTP to demonstrate that the power requirements are essentially the same. The power requirements for other parts of the science space-craft are not listed as they are assumed to be identical. It is therefore possible to conclude that the Pathfinder solar array of ~680 W of Pathfinder is sufficient for the needs of MAQRO.

Items & units LTP	**Power (W)**	**Items & units MAQRO**	**Power (W) CBE**	**Maturity Margin**	**CBE+Margin**
Inertial Sensor FEE	40	Accelerometer sensor Unit	4	5%	4.2
Charge Management (UV-lamps)	8	Accelerometer Control Unit	6	5%	6.3
Data and Diagnostic	30	Data and Diagnostic	30	10%	33
Phase-meter	18	Phase-meter +CCD	18	25%	22.5
Laser Assembly IR	45	Laser Assembly IR	45	10%	49.5
		Laser Assembly UV	20	25%	25
Total (science mode)	**141**	**Total (science mode)**	**123**	**average: 15%**	**141**
Total (maximal)	163	Total (maximal)	123	15%	141
Total (minimal, only DMU)	30	Total (minimal, only DMU)	30	10%	33
		Optional Heater for shields	105	20%	126
		Total (DMU+heater)	**140**	**average: 15%**	**159**

Table 6.3: The MAQRO payload power budget compared to the LTP power budget.

Note that a bake out mechanism for the outermost heat shield (+optical bench) can be optionally included for MAQRO. The heater requires ~105 W of power for bake-out at 300 K. Before commissioning, LTP and likewise MAQRO only requires 30 W of power so that the power difference of 110 W with respect to the LTP science mode are sufficient for bake-out. During bake-out only the experimental data management unit (DMU) and the shield heaters must be active.

Note that for bake-out at an ideal temperature of ~400K the required power is ~330 W. This is approximately twice the power budget allocated to LTP but it is still feasible if sufficient power from the science spacecraft can be temporarily allocated for the bake-out process

Table 6.4 gives an overview over the total power budget of LTP and MAQRO.

Payload Power required	**LTP**	**MAQRO**
Payload, maximal	163	159 (optional heater on)
Payload, Science Mode	141	141
Total Power required	**LISA Pathfinder**	**MAQRO**
Space-craft in Transfer Orbit	638	638
Space-craft in Science Mode	613	613

Table 6.4: the power budget for MAQRO payload and space-craft (third column) compared to the power budget of Pathfinder (second column).

6.3 Link Budget

Communication for MAQRO will be on X-band using low gain hemispherical and medium gain horn antennas, just as in Pathfinder. A communication bandwidth of 60 kbps fulfils the downlink bandwidth requirements for MAQRO. Therefore ~6W of transmitted RF-power are sufficient to establish the required downlink rate for on-station nominal operation. As in Pathfinder, it is suggested to use the 35 m antenna of the ground station Cebreros in Spain.

Operation mode	**Antenna**	**Downlink rate (ks/s)**	**Nominal TM margin (dB)**	**Uplink rate (ks/s)**	**Nominal TC margin (dB)**
On station nominal	Medium gain	120	10	2	38
On station emergency	Low Gain	1	10	2	20
LEO Phase nominal	Low Gain	120	36	2	71
LEO Phase w/c range	Low Gain	120	16	2	44

Table 6.5: The MAQRO link budget for various operation modes (from LEO transfer orbits to final L1 nominal operation).

6.4 Spacecraft thermal design

Besides the standard thermal control tasks, to keep the overall S/C and its external and internal units & equipments within the allowable temperature ranges by a proper thermal balance between isolating and radiating outer surfaces, supported by active control elements such as heaters, for the MAQRO mission the thermal design has to focus on a good thermal stability within the S/C (for CASE) and a proper thermal I/F design from the warm S/C to the extremely cold external payload DECIDE. The DECIDE S/C external experiment just by further de-coupling from a already very stable S/C and good coupling to a extreme stable 4 K environment can be kept at an extreme stable temperature.

IN order to achieve a good thermal stability for the CASE experiment, similarly to the LISA Pathfinder S/C, the MAQRO S/C internal dissipation fluctuations have to be minimized and the S/C interior has to be isolated from the solar array because it inherently introduces solar fluctuations into the S/C. In order to achieve the required 30 K environment at DECIDE, the (warm) mechanical I/F should be designed as cold as possible, e.g. 270 K, and the S/C surfaces facing towards the external payload should be covered by a high-efficient multi-layer insulation (20 layers) and the outermost layer should have a high emissivity > 0.8. This measure will serve for radiative pre-cooling of the outer thermal shield of the payload.

6.5 Attitude and orbit control

Star trackers and Solar sensor used to determine the attitude. The FEEPS (Field Emission Electric

Propulsion) are exclusively used for attitude control after the propulsion module has been ejected, i.e. there are no reaction wheels.

The attitude and control system (AOCS) for the science module is used whenever no science activity is carried out. It is referred to as MPACS on LPF, and can be used in a similar way for MAQRO. Likewise, a simplified version of the drag-free attitude and control system (DFACS) can be adapted from the more sophisticated Pathfinder concept.

6.6 Vacuum Requirements

The first missions which deal with rather stringent requirements on vacuum are LISA Pathfinder and LISA. In the former the vacuum is maintained inside a vacuum enclosure (inertial sensor) and the required pressure is 1E-6 Pa. In the latter a choice has been made not to use a vacuum enclosure around the experimental volume (which, in the case of LISA Pathifnder and LISA is a freely floating test-mass) but to vent to space instead and the required pressure is 1E-5 Pa (1E-7 mbar), which can be conveniently achieved after venting to space [24]. Based on previous studies for an alternative vacuum concept for LTP [25], we shall also use a "venting to space" to achieve a good vacuum of ~1E-7 Pa for the interior experiment (CASE) of MAQRO. Two aluminium tubes of ~10 cm diameter and 1.2 m length vent the molecular gases on the "cold side" of the space-craft, where the pipes pass the exterior heat shield and therefore avoid contaminating the DECIDE experiment. The feasibility of this concept from a vacuum as well as a thermal balancing and stability point of view has already been demonstrated in [25].

For the DECIDE experiment the vacuum requirements are much more stringent (1E-15 Pa). However, the temperature is also much lower and we found from analysis that outgassing is practically completely frozen out at such a low temperature. We shall briefly discuss the main results:

Quite generally, the ougassing rate $D_{out}[kg/s]$ is given by the following expression [24-26]

$$D_{out}(t) = m_{total} \times \sum_{species\ \mathrm{i}} \frac{TML_i(\%)}{100} \frac{e^{-t/\tau_i}}{\tau_i} \ , \qquad (6.1)$$

where τ_i is the outgassing time constant of molecular species i for a certain *material* of mass m_{total} and $TML_i(\%)$ is the total mass loss through outgassing of species i in percent.

In [25,26] an outgassing analysis for the Kompsat-2 mission has been performed from which outgassing rates for certain materials have been deduced. Typically every material outgases various molecular species with different outgassing time constants and total mass loss ratios. Those molecular species which outgas with very short time constants (on the order of a few hours up to some hundred hours) can be neglected. From the remaining molecular species the dominant ones are listed for three different materials in table 6.6

Material at 300 K	**Total mass loss (TML)**	**Outgassing time-constant**
Adhesive Scotchweld (EC2216)	0.558	12000
CFRP	0.207	2000
Kapton	0.0311	1.00E+04

Table 6.6: Outgassing rates of the dominant (on the mission timescale) molecular species for three different synthetics commonly used on a space-craft.

We shall define the particle emission rate γ_0 as the number of particles that are outgassed per time and per unit area from the surface of the plane. We deduce the emission rate from D_{out} by dividing

through the outgassing area A_{out} and the molecular mass m_i of the outgassed species i:

$$\gamma_0 = \frac{D_{out}}{m_i A_{out}}. \tag{6.2}$$

Assuming an infinite outgassing plane, it is a-priori plausible to assume, based on the ideal gas law, that the steady state density $n = N/V$, where N is the number of particles in the space-volume V, and the pressure P are given by

$$P = \gamma_0 \cdot m_i \cdot v_{rms} \qquad n_0 = \gamma_0 / v_{rms}, \tag{6.3}$$

where v_{rms} is the root-mean-square velocity of the gas molecules.

The product of mean density and mean velocity is given by the particle emission rate γ_0. The mean collision rate Γ_{coll} is given by

$$\Gamma_{coll} = n \cdot \overline{v} \cdot \sigma = \gamma_0 \cdot \sigma, \tag{6.4}$$

where $\sigma = \pi \cdot R_s^2$ is the interaction cross section and R_s is the radius of the sphere.

Taking the data from table 6.6 and considering the typical surface area of the components for which the outgassing was measured, we construct table 6.7:

Material	$D_{out}[kg \cdot s^{-1}]$	$m_{gas}[m_u]/\tau_i[h]$	$\gamma[m^{-2}s^{-1}]$	$P[mbar]$	$n = \frac{N}{V}[m^{-3}]$	$\Gamma_{coll}[s^{-1}]$ $R_s = 200\,nm$
CFRP	5E-9	30 / 2E3	48E14	7.1E-10	17E12	603
Kapton	4E-12	30 / 10E3	9E14	1.3E-10	3E12	113
Adhesives	9E-12	30 / 12E3	310E14	44E-10	108E12	3896

Table 6.7: Outgassing properties at 300 K for CFRP, Kapton and composite resins based on the data of table 4.1. The mass of the outgassed molecular species is assumed to be 30 atomic mass units. The calculated collision rate (column 6) assumes a sphere of radius 200 nm.

The outgassing rates in table 6.7 are applicable for an infinite surface at 300 K and are greatly reduced by two effects: geometric dilution and decreasing rates at lower temperatures.

Geometric dilution

As an example we shall first look at the outgassing from a sphere of radius R_{out} and an outgassing rate of γ_0 at its surface and then at the outgassing of a small surface element of area A_{out}. The two scenarios are depicted in Figure 3 and b, respectively.

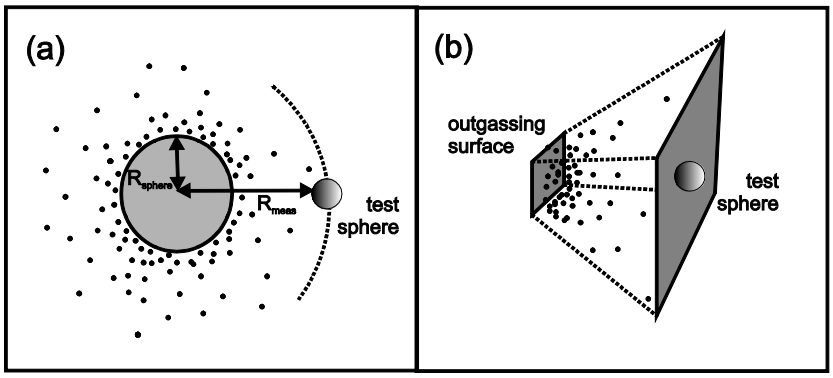

Figure 6.1: Outgassing froma sphere (a) and a quadratic surface element (b). In both cases the density of the outgassed molecules scales inversely proportional to the square distance.

The particle density $n(R_{meas})$ at a distance R_{meas} from the center of the outgassing sphere is given by the left expression in equation (6.5). The particle density $n(x_d)$ at a distance x_d from surface element

is given by the right expression, where we assumed that the distance between the outgassing surface element and the measurement sphere is much larger than the width of the surface element.

$$n(R_{meas}) = n_0 \frac{R_{sphere}^{\ 2}}{R_{meas}^{\ 2}} \qquad\qquad n(x_d) \sim n_0 \frac{A_{out}}{2x_d^2} \tag{6.5}$$

Based on equation (6.5) we find that for a typical scenario (e.g. Kapton fiber head, 1 mm diameter, 10 cm distant from microsphere) the densities/collision rates are suppressed by a factor of 3E-5., which greatly mitigates the outgassing rate.

Reducing the temperature

The temperature dependence of the outgassing time constants $\tau(T)$, also referred to as *residence times*, is generally given by the Arrhenius law, taken from [24-26].

$$\tau(T) = \tau_0 \cdot e^{\frac{E_A}{R_s T}}, \tag{6.6}$$

where $T[K]$ is the temperature, $R[J\,K^{-1}mol^{-1}]$ is the universal gas constant, and $E_A[J\,mol^{-1}]$ is the activation energy. We see that by increasing the temperature the outgassing process is exponentially accelerated and decreasing the temperature it is dramatically reduced.

Dynamic outgassing tests are performed at ESA/ESTEC with the purpose of quantifying outgassing and condensation of materials as function of temperature and time, to support mathematical models used for the prediction of molecular contaminant generation, migration, and deposition. Typically a Vacuum Balance Quartz Crystal (VBQC) is used in a standard program with 5 steps of 25 degrees to determine acceleration factors, temperature dependence of the residence time, and activation energy. VBQC outgassing kinetic tests at ESA/ESTEC usually show acceleration factors of between 3 and 10 for each 25° C temperature step.

The equation for the Arrhenius law (6.6) can be combined with the equation for the outgassing rate and the pressure (6.3) to yield:

$$P = \frac{D_{out}}{m_i \cdot A_{out}} m_i \cdot v_{rms} = m_{total} \frac{TML_i}{100} \frac{1}{\tau_i} \frac{v_{rms}}{A_{out}} = Const \cdot \sqrt{T} \cdot e^{-\frac{E_A}{R_s T}} \tag{6.7}$$

This equation gives the dependence of the pressure on temperature and can also be used to extrapolate the vapor pressure once the activation energy E_A is known. Note that the dependency on $\sqrt{T}$ can generally be neglected due to the very weak dependence on T compared to the exponential.

The acceleration factors between 3 and 10 which have been typically found in the ESA/ESTEC outgassing tests for various composite materials and resins, can then be used to calculate the activation energies $\tilde{E}_A$ per particle and we find $10\,E_{room} < \tilde{E}_A < 30 E_{room}$, where where $E_{room} = 300\,k_B$ is the energy associated with room temperature. From these typical activation energies of composite materials, we obtain the attenuation factors F_a for the outgassing rates (and therefore for the vapor pressure) when the temperature is reduced from 300 K to 30 K. We find that $F_a \sim 10^{40} - 10^{120}$, indicating that even materials which strongly outgas at room temperature have practically no outgassing at temperatures as low as 30 K (the temperature of the experimental volume in DECIDE). From fits of equation (6.7) to the data tables for vapor pressure provided in [27] we extracted the activation energies of various chemically inert refractory metals and found good agreement with those values found from field emission microscopy: $E_{Wolfram} = 140\,E_{room}, E_{Tantal} = 148\,E_{room}, E_{Noibium} = 128\,E_{room}$. The activation energies were used to extrapolate the pressures to very low temperatures. For these refractory elements the outgassing suppression is practically infinite.

6.7 The thermal Heat Shield

We propose a design of the heat shield that is based on experience gained from the "Darwin Proposal" and the Gaia mission. A schematic of the heat shield proposed for MAQRO is given in Figure 1 below.

The shield consists of three layers in the shape of either three cones or optionally, for ease of manufacturing, three pyramids in nested configuration. The vertex of the outermost cone is ~ 12 cm distant from the space-craft surface and there is approximately 5cm spacing between the vertices of the individual pyramids. The angle φ_P between the pyramid edge and the space-craft plane gradually increases from ~12° for the outer pyramid, ~24° for the middle pyramid, to ~36° for the inner pyramid. Such a design with varying opening angles improves the radiative cooling effect of the individual shields compared to a design with identical opening angles, giving each shield a greater solid angle for interaction and photon emission to deep space.

The shield structure is placed on the cold side of the space-craft where the propulsion module of Pathfinder is located. It is designed in such a way that it fits well into the inner space-craft cylinder to which the propulsion module is attached. The shields are gold coated on the underside (facing the space-craft) and have high emissivity (black coating) on the upper side facing deep space. The temperature of the space-craft outer surface (covered in MLI, outermost layer) is assumed to be 150 K-170 K), the surface temperature of the outer shield ~120K, of the middle shield ~70 K, and of the inner shield ~30-40 K. Note that the width of all shields is chosen sufficiently large so that no part of the "hot" space-craft surface is in direct line of sight with any optical bench component. The shield is mechanically attached to the 3 pairs of rods of a tripod which are fixed at the inner cylinder of the space-craft.

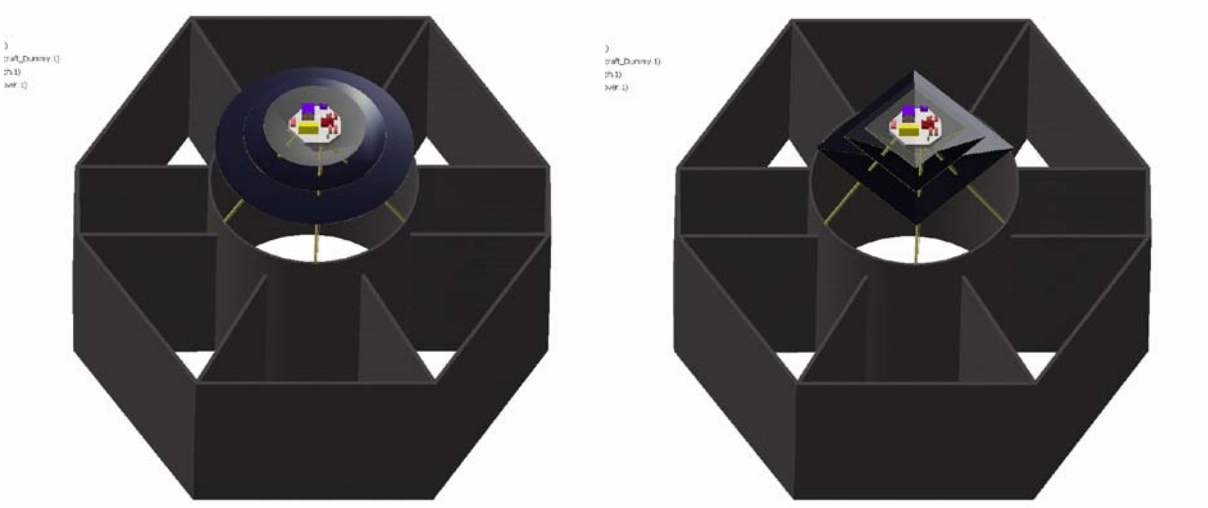

Figure **1: (a) A conical design for the MAQRO heat shield is attached to the inner space-craft cylinder of the LISA Pathfinder science platform. (b) For comparison a rectangular design is given.**

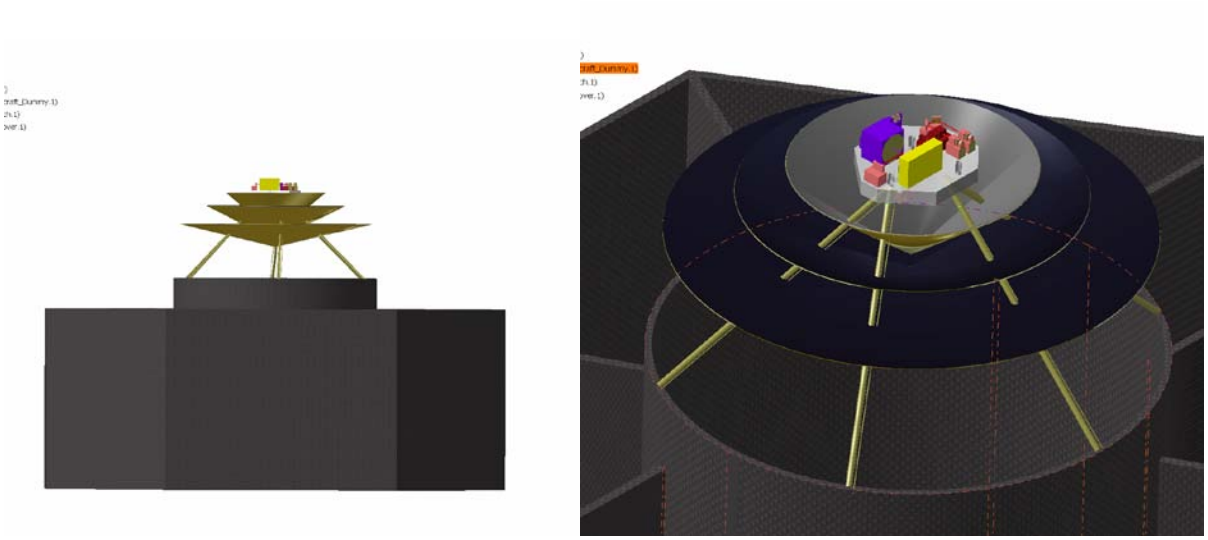

Figure 2: (a) Side-view of the heat shield visualizing the decreasing opening angles of the three shield layers and the geometric constraint that no part of the "hot space-craft" surface is in direct line of sight with the optical bench. (b) close-up of the heat shield with optical bench and components thereon.

The thick stable rods support the structure during the launch phase whereas the thin fragile rods which are drawn in parallel to the former ones support the structure after commissioning. Although the thick rods are built form a material of very low thermal conductivity (e.g. CFRP) their comparatively large cross-section –required for reasons of mechanical stability- is still conducive to heat transfer and limits the achievable temperature. To reach temperatures as low as 30 K it its therefore necessary to break the material and interrupt the thermal flow through it, which can be achieved by controlled release of a spring-mechanism, or a solution based on pyro-nuts as applied in the GAIA mission [28]. To minimize remaining effects of thermal photon emissivity which additionally deteriorate the thermal balance, the thick rods are covered by MLI with a low emissive finish. Note that the harness leading to/from the experiment (not drawn in figure) on the optical bench (2 IR glass-fibres, 1 UV glass-fibre, and 1 CCD sensor readout line) are either attached to one of the supporting rods or guided through one of the rods which is hollowed out for that purpose. More detailed analysis for the optimal concept is required.

6.7.1 Shield weight calculation

The area of the shield (all layers) is approximately $A_{shield} \sim 1 m^2$. For a first estimate we assume a specific density of $\rho \sim 2.7\, g/cm^3$ (aluminium) and a thickness of 1 mm which yields a weight of $m_{layers} \sim 3 kg$. Using a chemically inert and minimally outgassing refractory metal for the innermost shield, e.g. Tungsten or Niobium with $\rho_W \sim 19\, g/cm^3, \rho_{Nb} \sim 9\, g/cm^3$, would increase the weight to $m_{lyaers} \sim 3.7 - 4.7 kg$. The hollow struts are made from carbon-fibre reinforced plastics (CFRP) of very low thermal conductivity and expansion, as well as good mechanical stability. They are 40 cm long, 2 cm in diameter and have a wall thickness of 1.6 mm, giving a combined weight of less than one 1 kg: $m_{struts} \sim 0.6\, kg$. The struts are fitted to the bushings inserted into the base-plate of the optical bench. Each of the three inserts has approximately 200 g of weight giving a total of $m_{inserts} \sim 0.6 kg$. The struts are fixed to the space-craft inner cylinder by launch lock mechanisms. Each is estimated to weigh about 300 g giving a total of $m_{ll} = 1.8 kg$. The total weight for the shield with inserts and launch lock mechanism is approximately $m_{shield} \sim 7 kg$.

6.7.2 Protective cover, extendable shield, bake-out

During transfer to L1 and before ejection of the propulsion module the thermal shield is covered by an additional protective cover. The weight of the cover is estimated to be ~5 kg, based on an

aluminium cylinder with 0.8 m diameter, 0.16 mm wall thickness and a height of 0.5 m. In an alternative concept to the fixed and static shield depicted in Figures 1 and 2, a sliding shield could be extended from inside the inner space-craft cylinder through an extension mechanism.

Vacuum quality and outgassing is a key aspect of the coherence experiment. From our analysis we found that outgassing is practically completely frozen out at temperatures as low as ~30 K. Nevertheless, mainly as a means of risk mitigation for as yet unaccounted effects, it would be very useful to consider bake-out of the thermal shield and the exterior optical bench before commissioning. For that purpose heaters could be attached to the outermost shield and the optical bench. Considering that the outer shield area is approximately $A \sim 0.16 m^2$ and that the effective area of the optical bench $A \sim 0.07 m^2$, we obtain a total radiative surface of $A_{tot} \sim 0.23 m^2$ with an emissivity close to 1. This requires a heating power of P=105 W if we bake-out at 300 K and a heating power of P~330 W if we bake-out at 400 K.

6.7.3 Single mode fibre at cryogenic temperatures

From previous studies [29] we find that single mode glass fibres can in principle be operated at temperatures as low as 10 K without structural damage to the core. The study described in [23] deals with the design, manufacturing, and extensive testing of single mode waveguides in the mid-infrared for a typical Darwin application. Astrium investigated chalcogenide glass fibres that can be drawn by the double crucible method but mainly focused on extruded silver halide fibres made from AgBrCl. The environmental tests comprised a vacuum test at ambient, a cryogenic test at 10 K, proton radiation test, and gamma radiation tests. The fibre samples were coated with cladding mode absorbing layer on the cladding, multi-AR-layer coated at the facets, had PEEK protection tubes, and SMA connectors with ceramic ferrules. All performance tests were done at CO-laser wavelength of 5.6 micron and at CO2-laser wavelength of 10.6 micron within a Darwin representative interferometer. A major conclusion from the study is that the low temperatures cause no problem for the fibres themselves but the cooling process may damage the connector if materials with variable expansion coefficient are used to fixate the fibre core.

7 Science operations and archiving

7.1 Science operation architecture

Data for MAQRO are received by the 35 m Cerebros antenna in Spain and the routed to the European Space Operations Center (ESOC) in Darmstadt. The mission operations center (MOC) there ensures that the spacecraft meets its mission objectives, and it operates and maintains the necessary ground segment infrastructure.

In the L1/L2 there will only be 8h of ground station contact per day at a downlink rate of 60 kbps. The payload is commanded via Payload Operation Requests (POR) stored in the mission timeline. Real-time commanding only occurs during commissioning and contingency events.

If a highly-eccentric orbit is chosen, there will be an interruption of ground communication for several hours during passage through the perigee, which implies that there is never any ground station contact during the CASE experiment and all steps of the experiment have to be uploaded to the OBC.

The Science & Technology Operations Center (STOC), located in Madrid, is responsible for the planning of the payload operations, data analysis, and mission archive. Scientific advisors and investigators will collaborate with the core STOC team.

Volume requirements for data archiving and distribution are rather low for MAQRO. The total data received is estimated to be well below 300 GigaBytes, including diagnostic and house-keeping data.

7.2 Science data to be transmitted

Transmitted science data - DECIDE	
Type	**Description**
Results	
Particle position	Particle position reconstructed from spectrum (8 Bytes)
Particle position fit	Fit parameters to measured spectra (3 x 8 Byte)
UV beam position – CCD data	Center-of-mass determination of UV beam position from scattered light (4 x 8 Bytes – x-y position and x-y size)
UV beam position – Cavity readout	Estimate of UV position from cavity readout of particle position timed on scattered light detection with CCD (8 Bytes)
Particle temperature – longitudinal	Fit parameters to spectrum (6 x 8 Bytes) + estimated temperature (8 Bytes)
Particle temperature – radial	Diode readout (4 x 8 Bytes) + estimated temperature (8 Bytes)
Reserved	24 Bytes
Sub total:	**192 Bytes**
Diagnostic	
Particle number before manipulation	Number of particles in cavity mode as measured by CCD (2 Bytes)
Particle positions and widths	Results of center-of-mass particle-position determination from CCD image (4xNx8 Bytes – N: number of particles in cavity – typically: N=1)
Nr. of manipulation steps	Nr. of steps in manipulation until only 1 particle (2 Bytes)
Nr. of positioning steps	Nr. of steps for moving particle to experimental region (2 Bytes)
Nr. of experiment	Counter of performed experiments including this one (4 bytes)
Nr. of particle	Counter of successfully loaded particles including the current one (4 bytes)
Nr. of data runs	Counter of attempts to get a data point in the current experiment including the current attempt (4 bytes)
Nr. of successful runs	Counter of successful attempts to get a data point before the current attempt (4 bytes)
CCD intensity of UV scattering on state preparation	Scattering of UV light signals failure of state preparation – logging of CCD intensity for diagnostics (8 Bytes)
CCD intensity without UV scattering, cavity beam off	Background logging of CCD intensity for diagnostics (8 Bytes)

Status code	2 Bytes reserved (signals, e.g., loss of cavity lock)
Error code	2 Bytes reserved
Reserved space	24 Bytes
Sub total	**66 + 32 x N Bytes**
Total	**258 + 32 x N Bytes**

8 Technology development requirements

The TRLs for various components of the systems are listed in the tables of section 9.

9 Preliminary programmatics/costs

A description of the estimated costs for the proposed mission can be found in the tables below.

MAQRO Mission industrial costs incl.		Total
Phase B, C, D		**202300**
System level risk contingency	20%	40460
Phase E1 (Commissioning, Operations)		**3000**
Total		**245760**

Mission and System Prime		Total
Projekt Management		7300
Product Assurance		4100
System Engineering		20800
Satellite AIT		13500
Facilities and Support Equipment		6900
Total System Prime		52600

A more detailed key follows in the tables in the tables below.

Propulsion Module		Totals for Subsystem Parts Dev.+EM	QM/PFM	FM	Totals for Subsystem Parts Dev.+EM	QM	FM	Total	Risk		TRL at BCD Start	Comment
Structure		2200	2500	4000	100	0	2100	2200	low		TRL-9	Direct LPF heritage for all items
Thermal		600	700	1200	100	0	900	1000	low		TRL-9	
Separation System (PM/PM + PM/SC)		1100	500	1000	100	0	1000	1100	low		TRL-9	
Propulsion System		3500	5500	9300	300	0	5000	5300	low		TRL-9	
AOCS					100	0	2000	2100	low		TRL-9	
											TRL-9	
											TRL-9	
x-Band Communication System (Omnis)		300	400	600	100	0	800	900	low		TRL-9	
Harness		300	400	600	100	0	600	700	low		TRL-9	
MGSE		100	400	500		0	900	900	low		TRL-9	
Project Office, PA, SE, AIT, GSE		7700	5700	7400	100	0	2000	2100				
Total								**16300**	**k€**			

Spacecraft Bus Harware		Totals for Subsystem Parts							Risk	Current TRL	TRL at B/C/D Start	Comment
		Dev.+EM	QM/PFM	FM	Dev.+EM	QM	FM	Total				
Micropropulsion System												µN electrical Thruster or cold gas (Option)
	Micropropulsion	2000	4000	4000	2000	4000	4000	10000	low	TRL-6	TRL-7-9	LPF heritage with minor delta-development (ONERA Sensor interface)
Power					1000	0	4000	5000				LPF heritage
	Solar array (approx. 4 m2)		1600	1600					low	TRL-7	TRL-9	
	Battery (1 kWh -> 36 Ah @ 28V)	530	1330	1350					low	TRL-7	TRL-9	
	PCDU	500	1000	1000					low	TRL-7	TRL-9	
CDH					3500	0	3000	6500				LPF heritage
	OBC incl. operating system + drivers	2400	3000	4000					low	TRL-4-9	TRL-8	
	Remote Interface Unit	1100	900	1800					low	TRL-4-9	TRL-8	
AOCS					1300	0	5000	6300				LPF heritage
	Sun Sensor	300	360	720					low	TRL-9	TRL-9	
	Gyro Package	300	2600	5200					low	TRL-9	TRL-9	
	Star Tracker S/C	400	1500	3000					low	TRL-9	TRL-9	
	Star Tracker Prop. Module	300	600	1200					low	TRL-9	TRL-9	
Thermal					400	200	800	1400	low	TRL-5-9	TRL-9	Platform T/C LPF heritage
Communication Subsystem					3200	0	3500	6700				LPF heritage
	Transponder	1200	1750	3000					low	TRL-5-9	TRL-9	
	TWTA	500	750	1300					low	TRL-5-9	TRL-9	
	MGA incl drive	830	740	1250					low	TRL-5/6	TRL-9	
	Omni Antennas	440	480	800					low	TRL-5-9	TRL-9	
	Switches/Hybrids/Cables	170	360	630					low	TRL-9	TRL-9	
Structure including Interfaces					1000	0	2000	3000	low	TRL-5-9	TRL-9	LPF heritage
SCOE								2000	low	N/A	N/A	
MGSE								2500	low	N/A	N/A	
Harness					300	0	1200	1500	low	TRL-5-9	TRL-5-9	
Project Office, PA, SE, AIT, GSE								5000				
Total								**49900**	**k€**			

Payload DECIDE + CASE		Totals for Subsystem Parts Dev.+EM			QM		FM	Total	Cost Risk		TRL at BCD Start	Comment
Accelerometer sensor head								3000	low		TRL-9	ONERA
Accelerometer electronics								2000	low		TRL-9	ONERA
External vacuum and heat shield								3000	high		TRL-4	new development
DECIDE extension mechanism (Opt.)								4000	medium		TRL-5	use existing mechanisms/actuators (at warm side)
Shield backeout heater and power unit								500	low		TRL-5	use existing parts
Optical bench assembly DECIDE								10000	medium		TRL-6	based on LTP optical bench heritage
CCD + read out electronics								3000	high		TRL-5	major delta development
Particle dispenser								1500	high		TRL-3	new developmemt
Structural elements and cover								1500	medium		TRL-5	new developmemnt, but existing elements
Optical bench assembly CASE								8000	medium		TRL-5	
Structure, T/C and venting ducts								1500	medium		TRL-5	
Phasemeter								2500	low		TRL-8	
Laser Assembly (Infrared)								6000	medium		TRL-8	
Laser Assembly (UV)								7000	medium		TRL-6	based on UV LaserDiodes at 260 nm
Payload processor								3000	low		TRL-9	LTP processor
Ancillary sensors and electronic units								1500	low		TRL-9	LTP heritage
Harness								500	low			
Project Office, PA, SE, AIT, GSE								25000				
Total								83500				

10 Communication and outreach

MAQRO addresses the most basic and yet open questions of quantum theory. The appeal of its science mission to a general public is therefore obvious. Everyone has already heard about the famous “Schrödinger cat paradox” and many people will be interested to learn more about the fascinating discussions between Einstein, Bohr and Schrödinger and about the mind-boggling consequences of quantum theory for our world-view. This will guarantee MAQRO both maximum visibility and public interest from the very beginning.

Our communication program aims to reach out to a broad public audience by public lectures, interactive media (computer simulations, webpages, smart-phone applications etc.) and hands-on experience on table-top quantum experiments. At the same time, we will disseminate basics but also results of our current research both via public channels (webcasts, articles in the style of Scientific American etc.) and in high-profile scientific journals to also stimulate and rise the awareness of the broad scientific community.

11 References

[1] E. Witten, “Some properties of O(32) superstrings,” *Physics Letters B*, 1984, p. 5.

[2] E.G. Adelberger, B.R. Heckel, and A.E. Nelson, “Tests of the Gravitational Inverse-Square Law,” *Annu. Rev. Nucl. Part. Sci.*, vol. 53, 2003, pp. 77-121.

[3] D.J. Kapner, T.S. Cook, E.G. Adelberger, J.H. Gundlach, B.R. Heckel, C.D. Hoyle, and H.E. Swanson, “Tests of the Gravitational Inverse-Square Law below the Dark-Energy Length Scale,” *Phys. Rev. Lett.*, vol. 98, 2007, p. 21101.

[4] T. Damour, F. Piazza, and G. Veneziano, “Runaway Dilaton and Equivalence Principle Violations,” *Physical Review Letters*, vol. 89, Aug. 2002, p. 081601.

[5] P. Touboul, “MICROSCOPE, testing the equivalence principle in space,” *Comptes Rendus de l’Académie des Sciences - Series IV - Physics*, vol. 2, Nov. 2001, pp. 1271-1286.

[6] S. Schlamminger, K.-Y. Choi, T. Wagner, J. Gundlach, and E. Adelberger, “Test of the Equivalence Principle Using a Rotating Torsion Balance,” *Physical Review Letters*, vol. 100, Jan. 2008, p. 041101.

[7] S.G. Turyshev, “Experimental tests of general relativity: recent progress and future directions,” *Physics-Uspekhi*, vol. 52, 2009, p. 1.

[8] C. Everitt, “Historical perspective on testing the Equivalence Principle,” *Advances in Space Research*, vol. 32, Oct. 2003, pp. 1297-1300.

[9] T.J. Sumner, “The STEP and GAUGE Missions,” *Space Science Reviews*, vol. 148, Jul. 2009, pp. 475-487.

[10] P. Touboul, “Electrostatic space accelerometers for present and future missions,” *Acta Astronautica*, vol. 45, Nov. 1999, pp. 605-617.

[11] F. Karolyhazy, “Gravitation and quantum mechanics of macroscopic objects,” *Il Nuovo Cimento A*, vol. 42, Mar. 1966, pp. 390-402.

[12] G.C. Ghirardi, A. Rimini, and T. Weber, “Unified dynamics for microscopic and macroscopic systems,” *Phys. Rev.~D*, vol. 34, Jul. 1986, pp. 470-491.

[13] P. Pearle, “Combining stochastic dynamical state-vector reduction with spontaneous localization,” *Phys. Rev.~A*, vol. 39, 1989, pp. 2277-2289.

[14] L. Diósi, “A universal master equation for the gravitational violation of quantum mechanics,” *Physics Letters A*, vol. 120, 1987, pp. 377-381.

[15] R. Penrose, “On Gravity’s role in Quantum State Reduction,” *Gen. Rel. Grav.*, vol. 28, 1996, pp. 581-600.

[16] P. Pearle, J. Ring, J.I. Collar, and F.T. Avignone III, “The CSL Collapse Model and Spontaneous Radiation: An Update,” *Found. Phys.*, vol. 29, 1999, pp. 465-480.

[17] P. Rabl, C. Genes, K. Hammerer, and M. Aspelmeyer, “Phase-noise induced limitations on cooling and coherent evolution in optomechanical systems,” *Physical Review A*, vol. 80, Dec. 2009, p. 063819.

[18] S. Camatel and V. Ferrero, “Phase Noise Power Spectral Density Measurement of Narrow Linewidth CW Lasers Using an Optical Phase-Locked Loop,” *IEEE Photonics Technology Letters*, vol. 18, Dec. 2006, pp. 2529-2531.

[19] H.C. Hamaker, “The London--van der Waals attraction between spherical particles,” *Physica*, vol. 4, 1937, pp. 1058-1072.

[20] G. Ahmadi, “London-van der Waals Force,” 2006.

[21] T. Li, S. Kheifets, D. Medellin, and M.G. Raizen, “Measurement of the Instantaneous Velocity of a Brownian Particle,” *Science*, vol. 328, 2010, pp. 1673-1675.

[22] “e.motion (Earth System Mass Transport Mission), Proposal for Earth Explorer Opportunity Mission (EE-8), (October 2009).”

[23] “Notes and measurement data from Project ``Single-Mode Waveguide’', ESA Contract No. 20915/07/NL/CP, Start: 9th of October 2007, Expected end: January/February 2011.”

[24] “LISA-ASD-TN-3008, Peter Gath, ``Vacuum analysis’', issue 0.5, 27.03.2006.”

[25] “S2-ASD-RP-3016, Axel Hammesfahr, ``Study on Implementation of IS Vacuum Achievement by In-Orbit Venting’', issue 1, 24.10.2005.”

[26] H. Cho, \others, “``Measurement of outgassing from satellites’',” *Proceedings of the 5th International Symposium of Environmental Testing for Space Programs*, 2004.

[27] V.A.I. Inc., “No Title.”

[28] “GAIA-OSZ-DD-BRM-0001, Document from ``GAIA'', written by RUAG, issue 4.0, (30.10.2009).”

[29] “S2-ASU-MA-2020, Document from ``LISA Pathfinder'', Space-craft User Manual (Volume 4: AOCS), written by Astrium UK, issue 2,” 2010.